ABSTRACT

| | |
|---|---|
| Title of Thesis: | TOWARDS DEVELOPMENT OF A SPATIALLY-RESOLVED SPRAY SCANNING SYSTEM |
| | ***Stephen J. Jordan, Masters of Science, 2017*** |
| Thesis Directed By: | Associate Professor, Andre Marshall Ph.D., Fire Protection Engineering |

Fire sprinkler manufacturers have developed a plethora of application specific sprinkler designs. Advances in product development practices, performance based design, and fire suppression research have increased stakeholder interest in quantifying the spray produced by these devices. A Spatially-resolved Spray Scanning System (4S) has been developed to capture the complete spatio-stochastic nature of the droplets, which form sprinkler dependent spray patterns, at their point of origin. The 4S synthesizes spray measurements, transport analysis, and statistical representation frameworks providing high-fidelity spray characteristics suitable for evaluating both fire sprinkler and fire protection system performance. Terabyte scale data densities of 4S measurements present remarkable challenges with regard to data management, test repeatability, and test timing. These challenges are addressed through integration of automation, flow control, data acquisition and data analysis systems. Spatially-resolved sprinkler spray measurements are presented providing insight into the sprinkler spray patterns and their connection with deflector geometry, dispersion modeling, research and development.

# DEVELOPMENT OF A SPATIALLY-RESOLVED SPRAY SCANNING SYSTEM

by

Stephen J. Jordan

Thesis submitted to the Faculty of the Graduate School of the
University of Maryland, College Park, in partial fulfillment
of the requirements for the degree of
Master of Science
2017

Advisory Committee:
Professor Andre Marshall, Chair
Professor Marino diMarzo
Professor Michael Gollner

# Acknowledgements

Primary support for this project was provided by the National Science Foundation through a Major Research Instrumentation (MRI) grant, award number 1229506. The guidance of my academic advisor, Dr. Andre Marshall is most appreciated throughout the duration of this endeavor. Completion of this project was made possible through the support and guidance of colleagues, friends, and family: Noah Ryder, Eric Link, Taylor Myers, and Kathryn Staargaard. Several international collaborators helped advance the development of this state of the art measurement device and their contributions are appreciated: Juraj Repcik, Julian Zenner, Felix Fink, Valentin Uhlmann, Benjamin Burger, and Andreas Krieger.

# Table of Contents

# List of Figures

# List of Tables

# Nomenclature

| | |
|---|---|
| $A_{cyl}(\theta)$ | Total cross sectional areas of all cylinders at $\theta$, $cm^2$ |
| $A_{cap}(\theta)$ | Collection cap area calculated at $\theta$, $cm^2$ |
| $C$ | Rotation time scale constant, >1 |
| $c$ | Pressure transducer calibration, mv/mm |
| $D$ | Cylinder diameter, cm |
| $d_{v50}(\theta, \phi)$ | Volume median diameter, mm |
| $f$ | Laser imaging frequency, Hz |
| k | Sprinkler correlation between pressure and flow, $GPM/psi^{0.5}$ |
| $l_f$ | Low pass filter length, Hz |
| $N_{DPI}$ | Characteristics number of droplets captured per image |
| $N_{drops}$ | Number of droplets required for statistical calculation |
| $P_T$ | Pressure measured at the transducer, psi |
| $P_S$ | Set pressure for a measurement, psi |
| $P_{friction}$ | Pressure change caused by friction, psi |
| $P_{elevation}$ | Pressure difference caused by elevation change, psi |
| $P_{minor}$ | Pressure difference caused by minor losses, psi |
| $R$ | Line radius, m |
| $r$ | Initialization sphere radius, m |
| $T$ | Time from test initialization, s |
| $T_{rot}$ | Total rotation time, s |
| $t_{res}$ | Residence time of a probe at a measurement location, s |

| | |
|---|---|
| $t_{drop}$ | Time scale of droplet transport to measurement location, s |
| $u$ | Velocity, m/s |
| $\overline{u_0}(\theta,\phi)$ | volume weighted velocity, m/s |
| $\dot{V}_{spr}$ | Volume flow rate from sprinkler, $m^3/s$ |
| $\dot{v}''_S(\theta,\phi)$ | Volume flux through the initialization sphere surface, mm/min |
| $\dot{v}''_L(R)$ | Volume flux through plane below the sprinkler, mm/min |

**GREEK**

| | |
|---|---|
| $\Gamma(\theta,\phi)$ | Distribution parameter |
| $\theta$ | Elevation angle, degrees |
| $\rho$ | Density of water, $kg/m^3$ |
| $\phi$ | Azimuthal angle, degrees |
| $\omega_{rot}$ | Angular velocity of sprinkler rotation, degrees/second |

**SUBSCRIPTS**

| | |
|---|---|
| $m$ | Pertaining to mechanical sphere patternation |
| $o$ | Pertaining to optical sphere patternation |
| $probe$ | Pertaining to measurement probe |

# Chapter 1: Introduction

## *1.1. Motivation*

Water based, automatic fire protection systems are used world-wide to protect people and property from catastrophic fire losses. Each protection challenge, defined by the fire scenario and sprinkler system, relies on the effective dispersion of water from the activated sprinklers. Application driven design is common amongst sprinkler manufacturers; however, the number of unique sprinkler geometries dramatically exceeds the number of protection strategies available. The abundance of resulting spray patterns from these distinct sprinkler designs further complicates the challenge of predicting sprinkler system performance.

Most fire protection sprinklers share several primary structural components, as enumerated in Figure 1a, whose geometries define the spray characteristics. Following activation of the fire protection system, water ejected through an orifice (1); forms a jet that impinges on a conical boss structure (2); situated atop the deflector plate (3); and supported by a frame arm assembly. The reference frame arm (4); has been identified as a datum for measurement alignment and data synchronization. After the water jet strikes the deflector, distinct streams are created as the water flows along tines (5); and travels through open slots (6). These streams quickly disintegrate due to aerodynamic instabilities forming ligaments followed by a complicated distribution of drops as observed in Figure 1b.

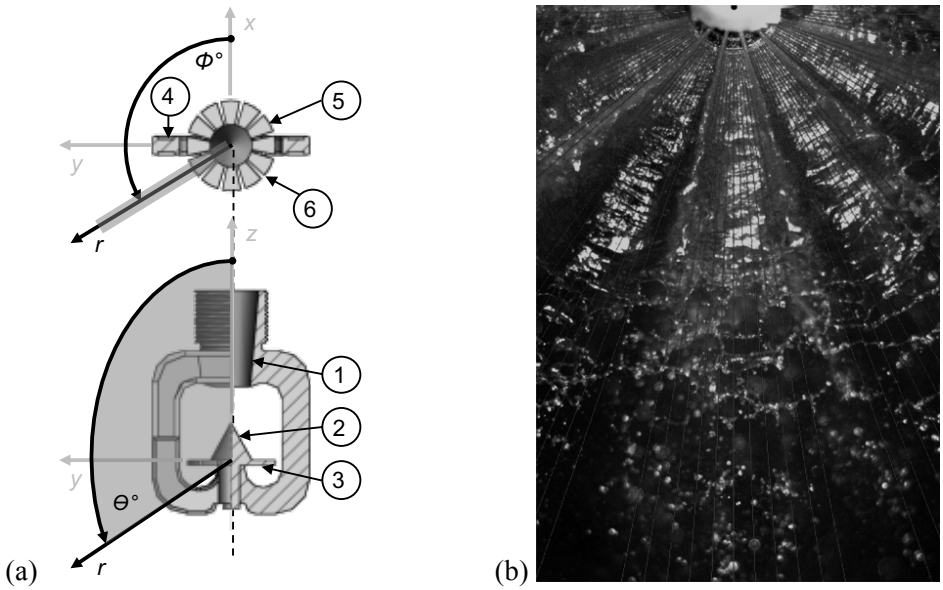


**Figure 1: Sprinkler and spray characteristics; (a) Sprinkler coordinate system and geometric features; (1) orifice, (2) frame arm, (3) boss, (4) deflector plate, (5) tine, (6) slot; (b) formation of droplets from the sprinkler deflector.**

It is clear from the body of work available on spray measurement and analysis that the spatio-stochastic nature of the spray favors statistical (over deterministic) treatment in determining the critical spray characteristics of drop size, velocity and volume flux [1]. In complex sprays such as those created by sprinklers, large quantities of drop realizations are required, locally, in order to accurately generate these statistical quantities. As the spatial fidelity of numerical simulations improves so too must the spatial resolution of spray measurements. Quality spray measurements, historically limited by the available measurement approaches, are pivotal to the development of new products, predictive models, and best practices within the fire protection and fire safety communities.

*1.2. Literature Review*

Spray measurements have evolved over the years according to analytical needs and available measurement techniques. Early measurement approaches for determining drop diameters included freezing droplets or capturing them with light oil [2]. These physical measurement techniques were phased out by the late 1980's with the introduction of optical measurement [3] and reverse spray modeling [4] approaches. Most notably, the complicated drop size distribution of a fire sprinkler was first measured with statistically sufficient detail by Yu [5] in 1986 using the FMRC Drop Size Measuring System. Yu confirmed the effect of pressure on drop size originally proposed by Heskestad in 1972 and the global effect of orifice size on drop size. This fundamental work established the combination log-normal Rosin-Rammler distribution still used presently to represent the drop size distributions observed for deflector based sprinklers. Despite the scientific advances in spray characterization near the turn of the century, numerical simulations of fire protection sprays by Bill [6] in 1993 and Nam [7] in 1996 were challenged to simultaneously implement a global drop size measurement and match experimental distribution data. These simulations lacked sufficient detail to fully describe the spatio-stochastic nature of sprinkler sprays.

In 2000, Sheppard [8] mapped experimental measurements to differential areas on the surface of a sphere surrounding the sprinkler in increments of 10 degrees. This work demonstrated the radial nature of drop velocity and the angular dependence of delivered density resulting from azimuthal variation in spray characteristics. Following the work by Sheppard, Walmsley and Yule [9] employed a photographic method to

characterize the drop size distribution formed from the slot, tine, and frame arm features of the sprinkler identifying the potential for further improved spray modeling with more detailed measurements. Local drop size measurements aligned with the slot and tine features were also conducted by Ren [10] in 2008 using a light diffraction technique for sizing and counting droplets. Volume flux measurements captured by Ren further demonstrated the distinctly different sprays formed by slot and tine streams as seen in Figure 2 and were applied to determine an overall flux-based drop size distribution. The results were observed to agree well with the distribution originally proposed by Yu two decades prior.

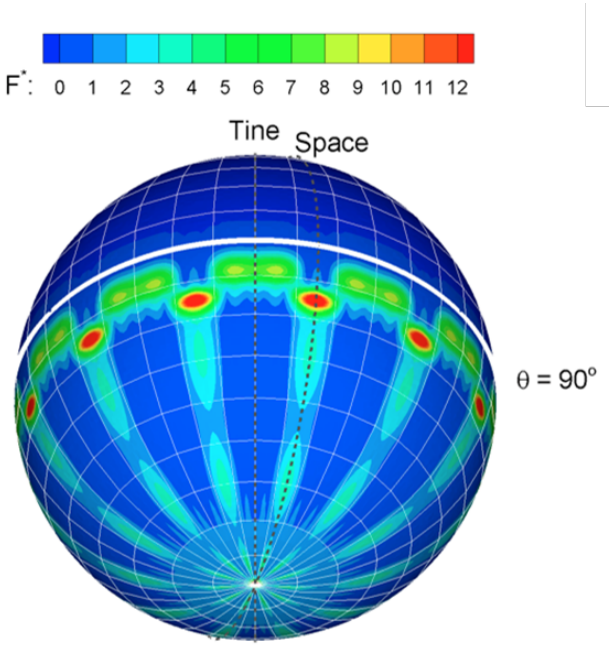


**Figure 2: Previous experimental work evaluated a single slot and tine formation in isolation assuming spray symmetry [11]**

Photographic measurement methods quickly evolved as the preferred approach for capturing spray characteristics. The non-intrusive nature of the optical technique

and the ability to simultaneously capture large quantities of multiple spray characteristics provide opportunities for reduced statistical error and increased spray insight [2, 12-15]. Applying a laser-based shadowgraphy imaging technique, Ren [16] captured nearly one million drop realizations to completely characterize the critical quantities of the spray in the form of probability distribution functions. Application of these measurements to spray initialization was further demonstrated to agree well with physical measurements of the spray [17]. Recent studies have employed a combined particle tracking velocimetry (PTV) and shadowgraphy measurement approach to spatially characterize all critical spray characteristics. Data compression methods developed by Ren et al. [16,18] further developed the analytical framework required to digest the large quantities of data gathered.

Measurements captured by Do [19] in 2009 of a pendent sprinkler are representative of the current labor-intensive methodology applied to spatial spray characterization. In the detailed stream-wise measurements conducted, drop sizes, velocities, and volume flux quantities were characterized for an idealized pendent sprinkler constructed of repeated slot and tine geometries. A discrete combined shadowgraphy and PTV measurement technique was applied with an imaging region measuring 150 mm x 150 mm in cross section, corresponding to a spatial resolution of nominally 0.1 mm per pixel. To characterize a single tine and slot stream, 19 sets of spray measurements were captured with each set consisting of 200 image pairs. The measurement regions were post processed individually to extract drop size and velocity

information and then stitched together, as shown in Figure 3, in order to gain a complete picture of the spray formed at a single slot and tine feature.

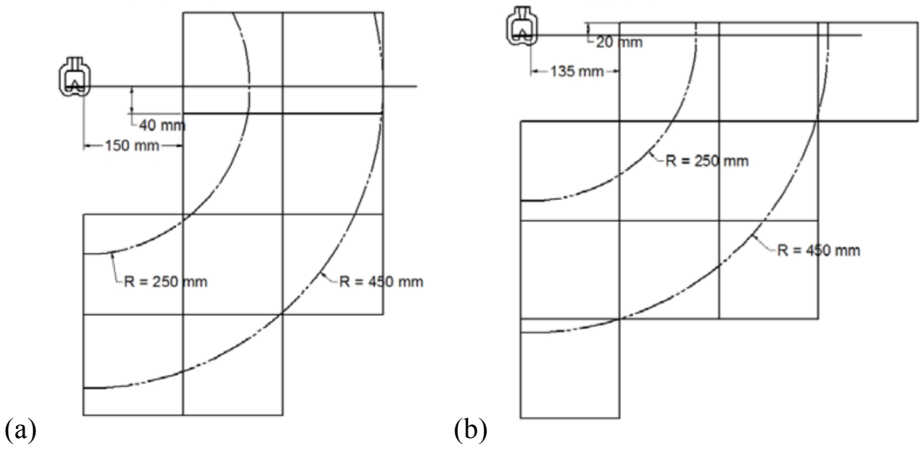


**Figure 3: Sprinkler spray characterization approach applied by Do [19]; (a) tine stream characterization; (b) Slot stream characterization**

Measurements by Do extended across three inlet pressures and four different nozzle orifice sizes for the tine flow and two orifice sizes at three inlet pressures for the slot flow. From the data collected, volumetric median drop sizes were calculated for each sprinkler pressure and orifice size configuration. A dimensionless characteristic drop size as a function of Weber number was observed to differ between the tine and slot centered flows measured. Although the measurements conducted in the study by Do were some of the most detailed near-field spray measurements conducted at that time, the results were limited to slot and tine centered spray characteristics occurring at 15 degree increments around the sprinkler. Further, the analysis conducted assumed a uniform drop size distribution across all elevation angles in the tine and slot streams, a step-change between the two flow streams types, and did not consider the effect of the frame arm structure.

Newly developed spray measurement techniques enable more accurate spray measurement and reproduction. By applying spray characterization methods similar to Ren and Do, Zhou and Yu [20] studied the effects of sprinkler geometry on spray characteristics including spray angle and droplet size in 2011. Most recently, modern spray measurement approaches were applied by Zhou in characterizing upright and pendent type ESFR sprinklers [21, 22]. These, and previous studies, demonstrate the feasibility of developing detailed spray characteristics through spatially resolved drop measurements and their utility.

Today's numerical simulations incorporating the detailed spatial dependence of the drop size and velocity distributions require extensive input parameters as identified by Myers [23]. Although the measurement techniques of late are capable of gathering large quantities of data, these approaches are still prohibitively expensive and tedious. The need for easily accessible, detailed, spatially-resolved spray measurements has led to the development of the Spatially-resolved Spray Scanning System (4S).

### *1.3. Research Objective*

The present research fills a gap identified in the measurement approaches applied to sprinkler spray characterization. Based on validated, proof of concept experimentation completed by Ren [10, 16], the construction of a next generation spray measurement device was initiated. Previous spray measurement approaches applied within the fire protection industry relied heavily on the test operator's expert measurement experience, lacking automation or versatility. As a result, specialized spray measurement approaches of this sort can be expensive to pursue outside of the

academic or laboratory environment. Through the synchronization of modern automation and adaptive spray measurement techniques, this research has produced the Spatially-resolved Spray Scanning System (4S), a state-of-the-art spray measurement device designed to provide easily accessible, highly resolved sprinkler spray measurements suitable for widespread adoption.

# Chapter 2: Approach

## *2.1. Overview*

The critical spray quantities identified in the body of work previously conducted, measured in this work with the 4S, provide a complete, spatially- resolved characterization of the sprinkler leaving nothing to guess about the initial spray formed. The 4S measurement approach facilitates data collection, reduction, and analysis through innovative experimental facilities and analytical approaches. Data reduction and analytical approaches are applied to the measurements to provide a complete, spatially-resolved characterization of the spray.

The experimental facilities developed are arranged into four main subsystems enumerated in Figure 4 and supported by automation, instrumentation, and data acquisition infrastructure. The flow control and sprinkler rotation system (1); establishes a well characterized inlet condition to the sprinkler prior to the formation of measureable drops and defines the measurement location relative to the deflector reference datum as well as the total measurement time. Physical measurements of the water delivered to both the mechanical sphere patternator (2); and integral line patternator (4); are generated to examine the volume flux through the surface of the initialization sphere, $\dot{v}''_S(\theta, \phi)$, and a plane below the sprinkler, $\dot{v}''_L(R)$. High resolution images of the spray captured by the optical sphere patternator (3); are evaluated to generate a representative drop diameter, $d_{v50}(\theta, \phi)$, drop size distribution parameter, $\Gamma(\theta, \phi)$, and reference velocity, $\overline{u_0}(\theta, \phi)$ at every measurement location.

The local spray measurements captured with each subsystem and used to develop the complete spray characterization are summarized in Table 1.

**Table 1: Spatially-resolved parameters calculated with 4S measurements**

| Subsystem | Parameter | Description |
|---|---|---|
| Mechanical Sphere Patternator (2) | $\dot{v}''_S(\theta,\phi)$ | Volume flux |
| Optical Sphere Patternator (3) | $d_{v50}(\theta,\phi)$ | Volume median diameter |
| Optical Sphere Patternator (3) | $\Gamma(\theta,\phi)$ | Distribution parameter |
| Optical Sphere Patternator (3) | $\overline{u_0}(\theta,\phi)$ | Reference velocity |
| Integral Line Patternator (4) | $\dot{v}''_L(R)$ | Volume flux |

## *2.2. Experimental Facilities*

### 2.2.1. Infrastructure

An enclosure constructed of extruded aluminum profile was built above a perforated, inclined floor used to collect and recirculate all discharged water. Spray dampening panels constructed from foam layers of increasing density are used to reduce satellite droplet formation and prevent spray penetration beyond the enclosure. The structure provides a level foundation and fixed alignment for the measurement systems as well as protected viewing area for test operation and observation. The 3-D rendering of the measurement device provided in Figure 5 shows the test chamber described as well as the identified spray diagnostic subsystems.

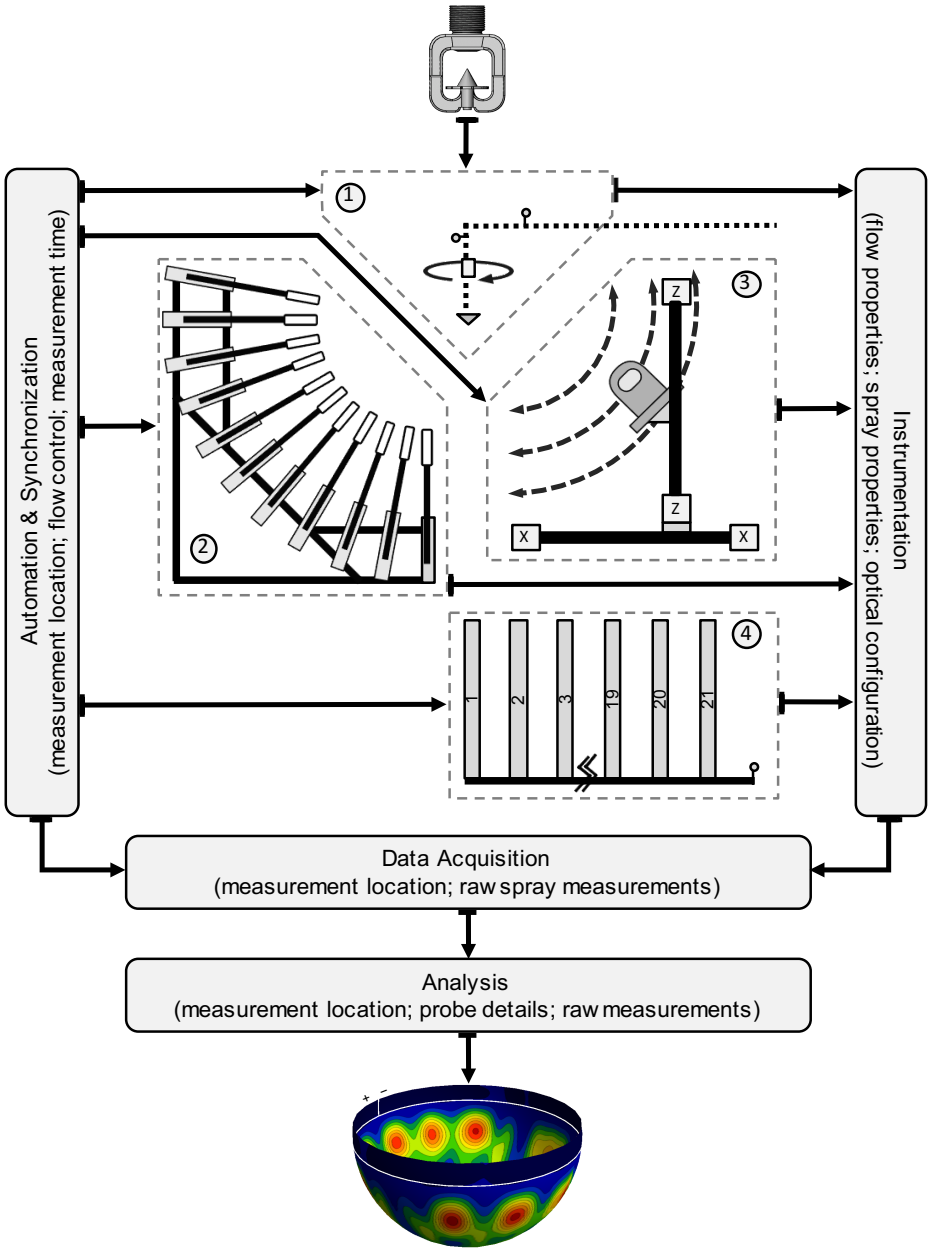


**Figure 4: Spatially-resolved Spray Scanning System (4S) measurement processes and subsystem elements (dashed regions); (1) flow control and conditioning; (2) mechanical sphere patternation; (3) optical sphere patternation; (4) integral line patternation.**

Integrating data collection capabilities with automation systems through highly regulated and strictly controlled automation approaches minimizes experimental uncertainty in measurement location and flow conditions in time. Spray measurement quality and speed were further improved by implementing automation algorithms for dynamic flow control and positioning of optical and mechanical sphere patternation measurements. A synchronized automation and data collection algorithm was also applied to the integral line patternation measurement subsystem to increase measurement speed and flexibility. All automation and data acquisition control components were built into a spray protected rack found adjacent to the observation window on the exterior of the 4S structure.

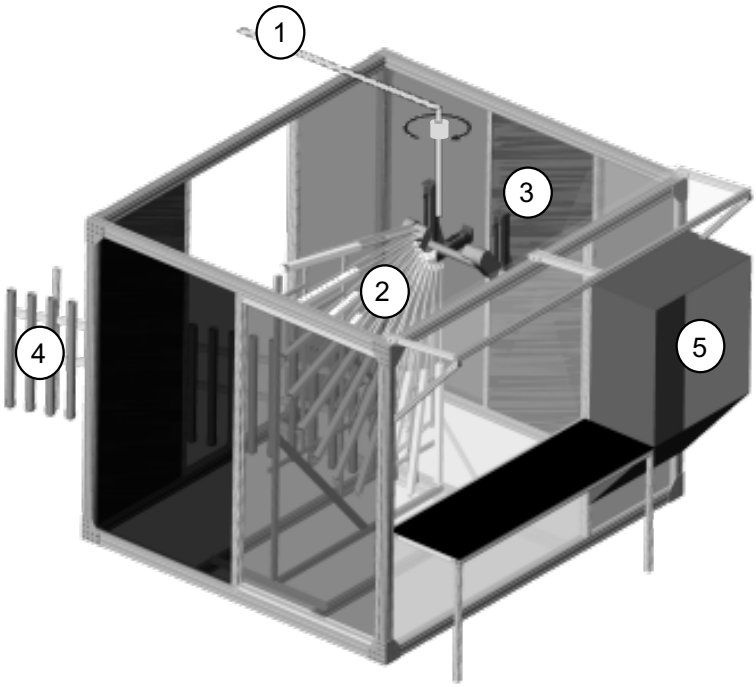


**Figure 5: Physical components of the 4S apparatus; (1) flow control; (2) spherical patternation; (3) optical patternation; (4) line patternation; (5) automation and data acquisition control.**

### 2.2.2. Flow Control and Sprinkler Rotation

The flow control and sprinkler rotation subsystem enables the automated 360° continuous rotation of the sprinkler while maintaining the prescribed inlet condition of sprinkler installed in the measurement device. Rigorous alignment of the sprinkler with the test apparatus is conducted for each sprinkler to ensure measurement repeatability and connect measured spray characteristics with the physical geometry of the sprinkler. Prior to the measurement of a sprinkler, the device is first installed into the 4S using the manufacturer recommended torque as listed on the product data sheet. The top of the deflector plate is then aligned in the same horizontal plane as the bisector of the 90° sampling tube and the centerline of the sprinkler orifice is aligned with the centerline of the 180° collection tube as shown in Figure 6a. The sprinkler is then azimuthally aligned such that the plane passing through the center of both frame arms is perpendicular to the center plane of the mechanical sphere patternator sampling region as demonstrated in Figure 6b. This installation orientation defines a $\phi = 0°$ azimuthal measurement datum at the mechanical sphere patternation plane, a $\phi = 90°$ datum at the reference frame arm, and a $\phi = 180°$ datum at the optical sphere patternation measurement plane. Based on this alignment the integral line patternator is positioned at the $\phi = 300°$ azimuthal reference location and fixed to the floor.

A vertical inline centrifugal pump provides water to the testing facility through a closed loop system designed to collect and recirculate all discharged water. A dynamic flow control system consisting of a parallel arrangement of two solenoid valves and one proportion valve was implemented to address the flow and pressure

limitations posed by a single speed pump configuration. The dynamic pressure at the centerline of the flow is measured above the sprinkler orifice and provides feedback for a proportional-integral-derivative (PID) control algorithm used to maintain a constant process pressure within ±2.5% of the set pressure based on measurements taken at a rate of 4 Hz during each test. The PID control settings applied were selected to balance the accuracy of the flow control system with response and recovery time to fluctuations in the supply flow. The measured process pressure was adjusted based on an effective distance between the measurement location and sprinkler orifice to account for pressure losses. A digital magmeter positioned in the supply line upstream of the pressure transducer provides a redundant measurement of the sprinkler flowrate. Corrected injection pressure measurements monitored and recorded for the duration of each test are the reported values of pressure presented throughout this analysis. For more information on the configuration of the flow control subsystem and hydraulic loss calibration the reader is directed to Appendix *A.1*.

During a 4S spray characterization, the sprinkler is slowly rotated at $\omega_{rot} = 0.02\ RPM$ throughout the duration of the test allowing for a continuous, three-dimensional scan of the sprinkler spray. Sprinkler rotation about the centerline of the orifice while maintaining a constant injection pressure minimizes the need to move sensitive spray measurement instrumentation. Stationary diagnostic equipment further increases measurement repeatability and accessibility while decreasing system complexity and cost. This approach provides a complete 360° view of the sprinkler spray unique to the 4S measurement approach. The rotation functionality is also used

during the alignment procedure to set the azimuthal zero datum prior to testing and enables integral line patternation measurements.

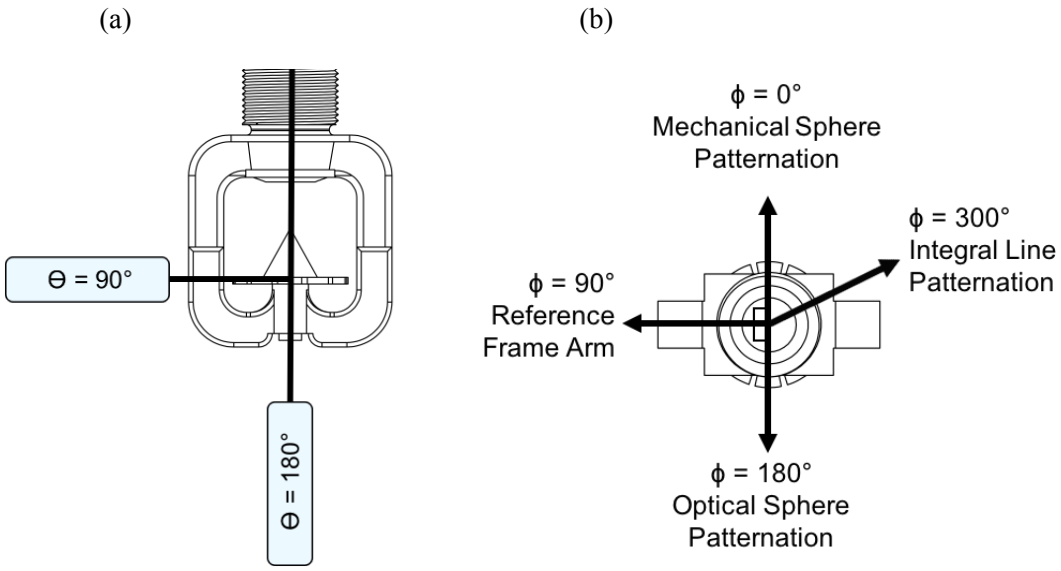


**Figure 6: Sprinkler alignment specifics; (a) Cartesian positioning alignment in XZ-plane [side view]; (b) rotation alignment around Z-axis [top view]**

### 2.2.3. Mechanical Sphere Patternation

Mechanical sphere patternation measurements are conducted to physically measure the spray pattern volume flux, $\dot{v}''_S(\theta, \phi)$. Eleven probes positioned at 10° increments between the elevation angles of $\theta = 80°$ and $\theta = 180°$ (south pole) collect and quantify the volume of water passing through each measurement region. The time rate of change in volume collected at each probe location is determined by physically storing all water captured over the duration of one test. Water height in the collection cylinders is continuously monitored using a Setra 209 pressure transducers attached to each cylinder array. A sample rate of 4 Hz was selected for the cylinder array pressure

based on previous measurement success over a dynamic range of 1 psig. The presented measurement accuracy of 0.25% corresponds to the full scale reading as provided by the manufacture and corresponds to a collected water height of approximately 1.7 mm of water.

With a series of automated linear actuators, the sprinkler spray examined in the 4S may be probed at radial distances measured from the center of the deflector over the range of

$$0.05\ m\ \leq r_m \leq 0.6\ m. \tag{1}$$

Previous experimental studies utilized this flexibility in measurement radius to investigate spray transport physics and validate early spray formation models. In this investigation a radial measurement location of 0.4 m was selected based on known sprinkler characteristics and previous experimental work.

For each test the collection cylinders were sized to optimize the measurement over the full dynamic range of the pressure transducer at each elevation angle. Sizes were selected to enable collection of all water delivered to the probe location throughout the test duration. To address the variability in flow distributions associated with different sprinkler classifications (e.g. ESFR, residential, sidewall, etc.) an array of 8 collection cylinders was constructed for each probe location enabling variable cylinder combinations with total cross-sectional areas of

$$1.96\ \text{cm}^2\ \leq A_{cyl}(\theta_m) \leq 985.4\ \text{cm}^2. \tag{2}$$

Measurement resolution and test duration are balanced to efficiently capture the spatial variations in volume flux unique to the different regions of a fire protection

sprinkler. Details of the cylinder areas applied are documented and used in post processing as described in the analytical approach section on mechanical sphere patternation. Water collection caps manufactured to fit on the end of the spray probes were applied to increase the effective probe area and resulting mass conservation over the spray measurement region.

The caps were designed to represent gore sections of the initialization sphere with a $(d\theta_m, d\phi_m) = (10°, 5°)$ consistent with the measurement resolution provided by the 11 probes in elevation as shown in Figure 7. Special consideration was given to the design of the caps near the equator and south pole based on the challenges of measurement lag time and minimum sample size. Further details on the mechanical sphere patternation measurement configuration, including an expanded discussion on the sizing of collection cylinders and collection caps, can be found in Appendix *A.2*.

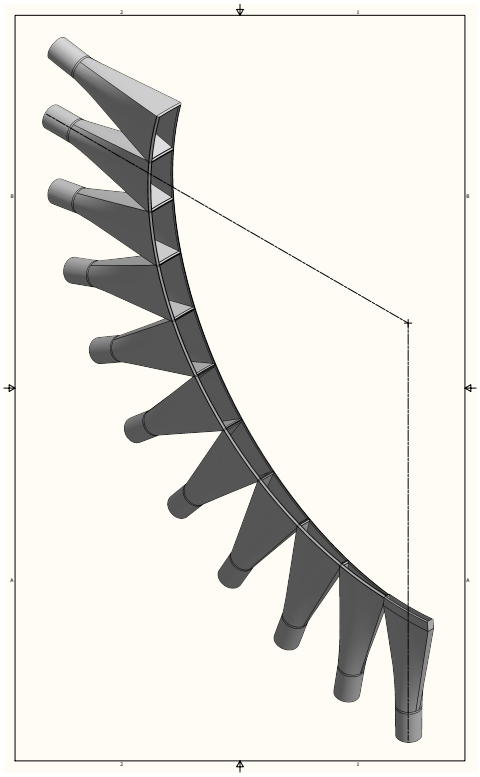

**Figure 7: Custom 3D printed collection caps**

### 2.2.4. Optical Sphere Patternation

A combined shadowgraphy and particle tracking velocimetry measurement approach was implemented into the 4S to optically measure local drop characteristics. The system utilizes a dual-cavity, frequency-doubled Nd:YAG laser producing 30mJ/pulse of 532nm light directed through a 50mm diffuser to produce an illuminated measurement field at a frequency of 6 Hz. Shadow representations of the sprinkler spray passing in front of the diffuser's illuminated field are captured with an ImagePro X 4M digital camera fitted with a 60 mm Nikon Micro-Nikkor f/2.8 lens aimed at the illumination field. The pulsed laser and camera are synchronized to provide double images of the drops separated by a time interval of 100 $\mu s$. The optical field of view in

this experimental setup was masked so only the illuminated region of the diffuser was preserved producing a 25 mm square field of view. The optical measurement was zeroed at $r_o = 0$ with the top, center of the deflector mid-frame. A 10 mm depth of field resulted from the selected field of view was centered so the tip of the sprinkler's boss feature was at the focal point of the image and in perfect focus. The optical measurement system was then positioned at the selected $(r_o, \theta_o)$ starting location prior to conducting the test. Spray protection fabricated to isolate the spray was installed to reduce satellite droplet formation and shield optical components.

The optical measurement system is integrated into the 4S workflow with automated positioning for

$$80° \leq \theta_o \leq 180°, \tag{3}$$

$$0\ m \leq r_o \leq 0.6\ m. \tag{4}$$

The measurement radius selected for this test series ensured that droplet formation was complete prior to passing through the sample volume as determined from previous measurements and drop breakup theory. A more throughout description of the optical alignment process is available in Appendix *A.3* with details on the design considerations applied to the curvature of spray protection.

### 2.2.5. Integral Line Patternation

Spray distributions delivered to a plane up to 1 m below the sprinkler deflector are measured using a linear mechanical patternator. During each measurement a series of 21 probes aligned radially from the centerline of the orifice is used to collect delivered

water over a complete 360° azimuthal exposure to the spray. Line patternation measurements are conducted over a known measurement duration typically following the rotation time applied to mechanical sphere patternation measurements. During investigation of the spray, water was allowed to accumulate in the 52.5 mm diameter measurement cylinders spanning radially from the sprinkler centerline at

$$0.3\ m\ \leq R \leq 3.2\ m. \tag{5}$$

Each cylinder was isolated from a common manifold by a valve to allow different levels of water to accumulate during the experiment. A pressure transducer located on the manifold connecting all collection cylinders is used to systematically measure the total accumulated volume at each radial location following the test. Recent developments have incorporated a normally closed solenoid valve in place of the manual ball values to enable automated line patternation measurements. Further details on the measurement process and experimental setup can be found in Appendix *A.4*.

### *2.3. Analytical Methodology*

A complete investigation of a sprinkler's spray characteristics with the 4S measurement approach results in a raw data set totaling on the order of 1Tb. Applying a series of analytical methods as described in this section, the raw data is reduced to a single spray characterization file on the order of kilobytes capable of statistically reproducing all spray measurements captured with the 4S. This master file provides all the information needed to reproduce the sprinkler spray in any analytical framework currently available.

### 2.3.1. Flow Control

*Theory*

The operating pressure of the sprinkler was measured during the experiment with the described pressure transducer configuration. The calibration of the set test pressure to the actual operating pressure of the sprinkler was conducted using a series of flow rate measurements over a range of pressures and sprinkler orifice sizes. The linear relationship between pressure measured at the transducer and the actual injection pressure was developed corresponding to the pressure losses through the pipe length and fittings and pressure head gained from elevation changes written as

$$P_S = P_T + P_{friction} + P_{minor} - P_{elevation}. \tag{6}$$

The associated calibration is valid for all testing conducted in the pendent orientation for a similar sprinkler orifice size. Maintaining a constant pressure, the continuous characterization taken around the spray is achieved by rotating the sprinkler slowly over the course of one measurement. From the time required to spin the sprinkler one complete revolution, $T_{rot}$, the angular velocity of the sprinkler is defined as

$$\omega_{rot} = \frac{360°}{T_{rot}}. \tag{7}$$

The azimuthal location of data collection can then be determined by the time stamp of the data collected relative to the total rotation time from

$$\phi = \omega_{rot} t. \tag{8}$$

*Parameters*

The rotation time is specified such that the time scales associated with spray dispersion measurement are sufficiently large compared to those of the sprinkler rotation. The

spray features associated with sprinkler deflector geometry are resolved by the mechanical and optical sphere patternation measurement subsystems by rotating sufficiently slow and generating a statistically significant quantity of unique volume flux or droplet realizations, respectively. The residence time of the measurement probe in the measurement region of interest is given by

$$t_{res} = \frac{d\phi_{probe}}{\omega_{rot}}. \tag{9}$$

The azimuthal width of the probe, $d\phi_{probe}$, is dependent on the measurement sub-system and thus at least two sprinkler rotation speed parameters will exist; the most stringent is considered the critical sprinkler rotation speed parameter and applied to the measurements collected. The minimum sprinkler rotation time required to appropriately resolve the gradients expected in the mechanical sphere patternation measurements was determined to be

$$T_{rot,m} = 1.8 * 10^4 \frac{\dot{V}_{spr} * \sin\theta}{D^2}. \tag{10}$$

As presented, the derivation of the equation is based on the geometry of the specific sprinkler analyzed and the minimum resolvable volume flux based on the measurement instrumentation of the mechanical sphere patternation subsystem as described in Section 2.2.3.

The minimum optical sphere patternation rotation time was determined based on the laser imaging frequency, $f$, a characteristic number of droplets per image, $N_{DPI}$, and a minimum number of droplets, $N_{drops}$, required to capture the droplet parameters

with statistical significance over the optical measurement region, $d\phi_{probe}$, as presented in Eq. (11). Use of this equation assumes that the laser frequency is sufficiently slow to refresh the droplet realizations measured in each image pair.

$$T_{rot,o} = \frac{360 * N_{drops}}{f * N_{DPI} * d\phi_{probe}}. \tag{11}$$

The critical sprinkler rotation time is presented as the maximum of the two calculated rotation times, Eq. (12). Measurements taken with sprinkler rotation times not exceeding the critical rotation time presented are subject to experimental errors beyond those addressed in Section 2.3.6.

$$T_{rot,critical} = Max[T_{rot,m}, T_{rot,o}] \tag{12}$$

2.3.2. Mechanical Sphere Patternation

*Theory*

Continuous flux measurements in the azimuthal direction for the eleven elevation angles probed are calculated based on the data collected from the mechanical sphere patternator and details pertaining to the experimental setup. Measurement data is collected as voltages sampled in time for each collection cylinder array. A low-pass filter of length $l_f$ is applied to the data to remove high frequency oscillations in the data consistent with electrical noise.

A first order technique was applied to evaluate the derivative of the measured voltage with a carefully selected time step, $dt$, corresponding to the minimum spatial resolution of the measurement. The voltage difference is then converted to a change in

water height, $dh$, over the time interval using a pressure transducer calibration factor, $c$, as

$$\frac{dh}{dt} = \frac{1}{c}\frac{dV}{dt}. \tag{13}$$

The ratio of cylinder cross sectional area to collection cap area at each elevation angle, $A_{cyl}/A_{cap}$, is applied to determine the local volume flux, $\dot{v}''_m(\theta, \phi)$, at a known position on the surface of the initialization sphere following

$$\dot{v}''_m(\theta_m, \phi_m) = \frac{dh}{dt}\,\frac{A_{cyl}(\theta_m)}{A_{cap}(\theta_m)}. \tag{14}$$

An interpolating function can be applied to gain insight into the spatial variations of volume flux at each elevation angle. Mass conservation is observed during the interpolation over each 10° measurement region based on physical spray measurements collected. The measured flux across the surface of the collection probes represents the cumulative effect of drop size, number, and velocity distributions. Typical convention in fire protection spray measurements is to represent the spray distribution as a delivered density in units of mm/min or GPM/ft$^2$. Following this standard, the spray is represented as a volume flow rate of liquid per unit area over the measured initialization sphere surface in a manner similar to that of Sheppard [24].

The volume flux represented on the initialization sphere should integrate to the sprinkler flow rate over the surface of the initialization sphere. Mass conservation and the quality of mechanical sphere patternation results can be evaluated using the theoretical flow rate calculated from the sprinkler k-factor and test pressure. Details of

the mass conservation analysis conducted on the mechanical measurements collected are provided in the error analysis discussion of the results section.

*Parameters*

A number of user-defined parameters are used to calculate the volume flux over the surface of the initialization sphere; some based on the measurement configuration and others on developed measurement theory. The first parameter used in the process was the filter length applied to the low pass filter which was conservatively short to avoid reducing the spatial resolution of the measurement following

$$l_f < t_{res}. \tag{15}$$

In calculating the first order derivative of height with time within the cylinders the calibration coefficient used calculated from the voltage output and pressure range for the pressure transducer. This calibration coefficient was verified with known volumes of water when commissioning the device. The *dt* used was a fraction of the overall probe residence time sufficiently short to provide several measurements across the azimuthal arc length of the probe cap yet long enough to provide an average of the flux over the slowest spray fluctuations. If probes of identical size were used in all elevation angles, the time used in this analysis would vary by elevation angle and be proportional to the resonance time of the probe and a function of the probe width. However, for these experiments the collection caps were designed to probe the spray with a width weighted by $\sin\theta$ such that collection caps located near the equator were larger than caps located closer to the pole. As a result of this design modification, use of a single *dt* is sufficient for this analysis.

To relate the apparent flux within the collection cylinder to the flux on the surface of the initialization sphere the area ratio of the cylinder to collection cap is utilized at each location. These values are calculated from the experimental configuration as

$$A_{cyl}(\theta_m) = \sum_{i=1}^{n} \frac{\pi}{4} D_i(\theta_m)^2, \tag{16}$$

$$A_{cap}(\theta_m) = \iint {r_m}^2 \sin\theta_m \, d\theta_m d\phi_m. \tag{17}$$

It should be noted that the cylinder area is calculated as the total of all open cylinders at the measurement location and should include the area of the supply tube used to feed the collection cylinder manifold. Future work will focus on the detailed development of the measurement theory for the various 4S subsystems and include a thorough investigation of the mechanical measurement resolution possible given a set of test parameters.

### 2.3.3. Optical Sphere Patternation

*Theory – Image Processing*

Images of the droplets captured during the spray characterization total more than 250,000 frames and constitute a majority of the data volume. Image pairs were analyzed using a pixel counting algorithm and reduced to particle lists containing detailed information on position, size, and velocity for each measurable droplet identified in the images. For each image pair captured, several steps are taken before droplet characteristics can be extracted: frame filtering and inverted (1); reference image

calculation (2); particle segmentation and measurement (3); and velocity vector calculation (4).

1. Frame Filtering and Inversion:

Each frame of the image pair is filtered to reduce noise using a 3x3 average filter to smooth dead and oversaturated pixels from the image. The minimum intensity of the image is then subtracted from all pixels. An inverted image, like the one shown in Figure 8a, is generated by subtracting the preprocessed image from a calculated reference image.

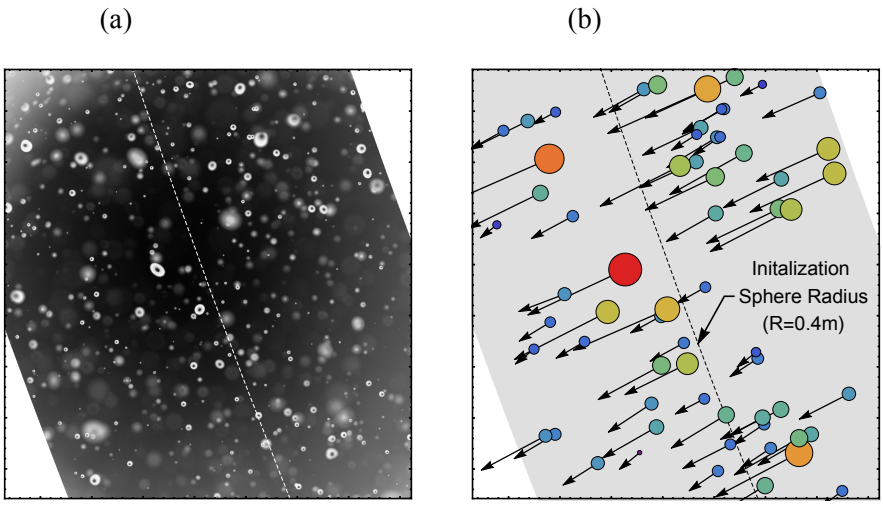


**Figure 8: Shadowgraphy optical measurement technique; (a) raw composite image of the droplets; (b) processed image used to obtain drop size and velocity characteristics [25].**

2. Reference Image Calculation

The reference image is calculated for each frame by applying a strict sliding filter with a defined pixel width to the image. This strict sliding maximum filter searches the domain of the filter returning the maximum; effectively removing the particles from

the image. Image pixel intensities are subtracted from the calculated reference image values. The calculated difference is then normalized by the reference image, an additional step recommended to minimize systematic errors caused by non-uniform illumination between frames and image pairs [26].

3. Particle Segmentation and Measurement

Once the frames are inverted a two phase segmentation is applied to extract droplet size information. First a global segmentation is applied based on a user defined global threshold value. A bounding box is then generated around adjacent pixels with intensities above the global threshold defining potential initial particle locations. A minimum shadowing specification is applied to prevent noise characterization in the event that no particles are captured in the image.

A second particle segmentation process fits rectangular masks to enclose the image regions identified in the first segmentation and expanded based on an area of expansion parameter. These regions are extracted for further evaluation. High and low level threshold percentages are applied to determine particle statistics including diameter, centricity, and location as calculated from the average of the values determined with the two threshold values. The pixel length scale calibration is applied to get drop size measurements and identified particles are filtered based on clarity, size, position, and shape before being tabulated in a particle list file according to image and frame number. Following particle segmentation, the identified drops in the two frames of each image pair can be linked.

4. Velocity Vector Calculation

Only once a particle has been identified in both frames is a velocity calculated and included in the detailed particle list. To locate the partner drop from the second frame of the image pair, a search window is applied based on an anticipated velocity vector. User defined parameters for the particle size deviation and shift tolerance between the two frames are used to identify droplet pairs from which the particle velocity can be calculated. After processing the image shown in Figure 8a, the drop size, position, and velocity information obtained was used to generate Figure 8b. The drop representations and velocity vectors shown are scaled based on measured drop size and velocity respectively.

*Theory – Particle List Processing*

Spray statistics for all droplets passing through the surface of the initialization sphere were generated from parsed particle list files and measurement position data. Of interest to the specification of the initial sprinkler spray are the volume median diameter of the droplets, $d_{v50}(\theta, \phi)$, and the width of the drop size distribution, $\Gamma(\theta, \phi)$, which corresponds to the local spray uniformity. Together, these parameters define the drop size characteristics formed at each azimuthal and elevation angle. From the list of particles at a given location having drop diameters, $d$, the values of $d_{v50}(\theta_o, \phi_o)$ and $\Gamma(\theta_o, \phi_o)$ are simultaneously calculated using the combination log-normal and Rosin-Rammler distribution fit to the cumulative volume fraction of the local spray with

$$CVF(d) = \begin{cases} \dfrac{1}{\sqrt{2\pi}} \displaystyle\int_0^d \frac{\Gamma}{1.15d'} \exp\left( \frac{-\ln\left(\frac{d'}{d_{v50}}\right)^2}{2\left(\frac{1.15}{\Gamma}\right)^2} \right) dd' & d < d_{v50}, \\ 1 - \mathrm{e}^{-0.693\left(\frac{\mathrm{d}}{\mathrm{d_{v50}}}\right)^{\Gamma}} & d > d_{v50} \end{cases} \tag{18}$$

For traditional fire protection sprinklers, $d_{v50}$ varies between 0.5 and 3.5 mm and Γ is commonly found to be between 2 and 4 [23]. A larger value for Γ indicates a less uniform spray distribution at a given location while a larger characteristic $d_{v50}$ within the given spray indicates the presence of larger droplets on a volumetric basis.

The characteristic initial velocity of the local spray, $\overline{u_0}(\theta, \phi)$, is also calculated based on drop measurements. A volume weighted velocity is typically used to represent the bulk spray velocity at each location. Details pertaining to a local drop diameter-velocity correlation at any given location are also available from the data collected in a typical spray characterization. The velocity used in this analysis was calculated from

$$\overline{u_0}(\theta_o, \phi_o) = \frac{\sum {d_i}^3 u_i}{\sum {d_i}^3}. \tag{19}$$

*Parameters*

Optical measurements were captured at a measurement radius sufficiently large to ensure that droplet formation was completed prior to passing through the probe volume defined by the depth of field and the field of view. The minimum optical measurement radius is known to be inversely proportional to both pressure and sprinkler orifice size and will vary based upon test conditions and sprinkler size [5].

Once all images from the measurement are captured, the post-processing of each image begins with the calculation of a reference image. For the strict sliding

maximum filter applied, the filter length selected should be at least 1.5 times the largest particle expected. The maximum measurable droplet size in this analysis, based on the selected filter of 400 pixels, is nominally 4 mm in diameter. To identify the particle regions in the global segmentation a global threshold parameter is called which represents a percentage of the difference between the maximum and minimum pixel saturation values in the inverted image. The particle search algorithm in this first segmentation is limited to regions above the global threshold set at 50% for these measurements.

The regions identified from the global segmentation are expanded based on the 50% area of expansion parameter defined and fed to the second segmentation process. High level (60%) and low level (30%) threshold percentages corresponding to the range of pixel intensities are used to evaluate drop size. Particle statistics are then generated if the identified droplet passes several filters applied to limit the measured optical noise. A minimum particle area, defined as 16 pixels, filters out unwanted satellite droplets corresponding to droplets with diameters smaller than approximately 0.08 mm. Particles touching the boarder of the image frame or having a centricity less than 40% were also excluded in this analysis.

A final filter is applied based on the ratio of drop areas calculated from the low and high thresholds. Particles that are closer to the focal point of the lens create a sharper contrast on the illuminated background and have a smaller ratio. Defining a maximum low level area percentage as 150% of the area calculated using the high level

threshold sets the minimum boundary definition or clarity required for a counted particle.

To calculate the velocity a shift parameter is required and defined as the shift in the x and y coordinate of a particle from one frame to the next. The anticipated shift applied in this application was a function of the test pressure, $P_S$, measurement location, $\theta_o$, and time step between frames in an image pair, $dt_l$, defined during image acquisition.

$$|\overrightarrow{u_0}| \approx 0.7\sqrt{\frac{2P_S}{\rho}} \tag{20}$$

$$(dx, dy) = (-|\overrightarrow{u_0}|\, dt_l \sin\theta_o\,, -|\overrightarrow{u_0}|\, dt_l \cos\theta_o) \tag{21}$$

The time step between frames should be selected to ensure that particles move a minimum of 3 pixels plus one half the smallest drop size anticipated from one frame to the next. A Large shift between image frames improves the accuracy of the velocity calculation but decreases the number of valid velocity realizations since a single particle must be visible in both frames. As spray density decreases larger shifts become more feasible however identification of the correct drop partner must be maintained. A search window of 2 x 2 mm centered on the shifted position in the second frame was applied to identify drops within the allowable drop size deviation of 15%. Only once a particle has been identified in both frames is a velocity calculated and included in the detailed particle list.

### 2.3.4. Integral Line Patternation

*Theory*

Integral line patternation measurements are collected from the pressure transducer as raw voltages. From this data, an average radial profile for the volume flux of water passing through a surface 1 m below the sprinkler can be calculated. The volume of water accumulated in the 21 collection cylinders is calculated from a baseline measurement pertaining to a uniform height of water across all cylinders at the beginning of the test. For each radial probe the change in voltage from the baseline water level measurement, $dV_R$, is calculated over the test duration $dT_{rot}$ and related to a pressure. The net pressure is converted to a total accumulated volume of water in each cylinder based on the area ratio of the collection cylinder to cylinder cap, $A_{cylinder}/A_{cap}$. The average flux delivered to a probe positioned at a radial distance, $R$, from the centerline of the sprinkler can be calculated as

$$\dot{v}''(R) = c\frac{dV_R}{dT_{rot}}\frac{A_{cyl}(R)}{A_{cap}(R)}, \tag{22}$$

where the constant, $c$, represents the calibration of the pressure transducer in millivolts per measured millimeter of water height.

Using the complete spray characterization provided by 4S measurements, spray dispersion to a horizontal plane 1 m below the sprinkler can be modeled using CFD simulations or first order Lagrangian particle tracking algorithms developed for rapid spray visualization. From the results of these simulations azimuthal mean volume fluxes can be compared to integral line patternation measurements as a function of the radial coordinate. Comparison of dispersion measurements and 4S measurement based

predictions in the results to follow demonstrate proper specification of the initial sprinkler spray.

*Parameters*

The experimental configuration selected for this test series did not utilize caps or funnels to alter the effective collection area of the line patternator cylinders. All collection cylinders used were sized at $D_R$ = 52 mm with an effective area ratio of one. Average delivered flux was calculated directly from the average time rate of change in water height within the cylinders. The pressure at the start of the test was determined by the reset drain level as measured across all cylinders and used as the baseline pressure in determining a $dV_R$ for integral line patternation measurements.

### 2.3.5. Experimental Scope

In this evaluation, a fire protection nozzle typical to several industrial fire protection deluge applications was evaluated at a pressure of 19.7psi using the 4S measurement apparatus developed. Mechanical sphere patternation measurements were conducted in parallel with both optical sphere patternation measurements and integral line patternation measurements to fully characterize the spray formed by this nozzle. Mechanical sphere patternation measurements were repeated several times to generate statics on repeatability and provide a robust measurement set for validation of the flux calculated from optical measurements of the spray characteristics. The implementation of the outlined analytical approaches to these measurements results in a spatially-resolved characterization of the spray formed by the nozzle of interest.

### 2.3.6. Error Quantification

Error analysis is conducted to quantify the error associated with the measurements presented. The quality of the data collection approaches applied is generalized by examining both the repeatability of the measurement process and the spray itself. The experimental results were developed based on several generalized assumptions for parameters related to the measured spray, including the anticipated time scale of the slowest spray pattern fluctuation. The error analysis applied to the system demonstrates the validity of these assumptions and the overall quality and reproducibility of the individual spray measurements and comprehensive 4S sprinkler characterization.

The presented error analysis is not an exhaustive analysis into error quantification. For a system of this scope, potential sources of error are numerous and include: measurement alignment errors related to sprinkler installation procedures; measurement uncertainties associated with experimental setup and collection cylinder configuration; flow instability errors; measurement parameter selection errors from improper application of the measurement theory; and instrumentation and diagnostic errors. In this work, measurement theory errors pertaining to the selected measurement parameters are addressed in Section 2.3.1 while analysis of the repeatability error for select 4S diagnostic equipment is presented in Section 3.2 for sprinkler rotation automation and mechanical flux measurements. Optical sphere patternation measurement error was not directly characterized; however, measurements were conducted with similar experimental and post processing parameters to studies conducted by Ren [11] who observed optical spray measurement accuracies within

±5%. The optical sphere patternation measurements presented are thus anticipated to present a similar error at less than ±5%.

# Chapter 3: Results

## *3.1. 4S Measurements*

Nearly 1Tb of spray information was collected in the spray measurement approach applied to the spray characterization presented. A reduced dataset containing the detailed statistical distributions required for reconstruction of the measured spray is presented in terms of volume flux, volume weighted drop velocity, volume median drop size, and the distribution parameter for every position across the initialization sphere surface. Each of the parameter specific data subsets are represented in Figure 9 on the initialization surface over which the measurements were collected. The collective set of data shown represents everything there is to know about the spray formed from the measured fire protection sprinkler.

Measured volume flux over the surface of the sphere is shown in Figure 9a with a district pattern of tine and slot flow formations visible around the sprinkler. The white horizontal band around the sphere represents the equator of the initialization sphere with a radius of 0.4 m and further identifies the 90° elevation angle location. A white vertical bar has also been placed on the figure to indicate the 0° azimuthal datum with the positive and negative indices shown. Consistent with the measurement orientation shown in Figure 6b, the reference frame arm is located at $\phi = 90°$.

Measured volume flux is a compound effect of drop volume median diameter, Figure 9b, and the volume weighted velocity, Figure 9c. The observation of larger drop sizes and velocities for the tine formations near the equator and slot formations near

the south pole are consistent with the higher flux values measured at these locations. The distribution of gamma values shown in Figure 9d demonstrates that calculated values of gamma are primarily consistent over regions of measurable flux and that areas of higher drop density have a slightly more consistent drop size distribution than low density regions. As presented, the mechanical and optical sphere measurements correspond to the same reference geometry on the sprinkler; all optical measurements have been adjusted to align with the mechanical sphere patternation measurements such that

$$\phi = \phi_m = \phi_o + 180°. \tag{23}$$

From the presented set of data, the non-homogeneous tendencies of the measured spray parameters are apparent. Detailed investigation of the parameter span visually represented in Figure 9 demonstrates a large variance from both the statistical and surface area weighted mean values. The 5% and 95% quantiles for the spray parameters were selected to represent the span of the values measured for each parameter and are compared to the calculated mean approximations, Table 2. The standard deviations of the parameters over the surface of the initialization sphere were determined to range from 18% to 72% of the statistical mean further indicating large spatial variations.

**Table 2: Non-homogeneous nature of spray parameters**

| Parameter | 5% Quantile | | 95% Quantile | | Mean Approximation | |
|---|---|---|---|---|---|---|
| | Value | Location | Value | Location | Statistical | Weighted |
| $\dot{v}''_S(\theta,\phi)$ [mm/min] | 0.01 | (80; 120) | 89.2 | (170; 170) | 39.0 | 33.0 |
| $d_{v50}(\theta,\phi)$ [mm] | 0.4 | (80; 50) | 0.84 | (170; 80) | 0.6 | 0.57 |
| $\Gamma(\theta,\phi)$ | 2.2 | (130; 100) | 4.0 | (110; 95) | 3.24 | 3.34 |
| $\overline{u_0}(\theta,\phi)$ [m/s] | 3.75 | (80; 50) | 9.8 | (140; 150) | 7.19 | 7.51 |

3.1.1. Mechanical Sphere Patternation

The measured volume flux as captured with the mechanical sphere patternator is represented on the initialization sphere shown in Figure 9a. The observation of high flux regions measured near the 110° elevation angle and centered at 30° intervals is consistent with the orientation and frequency of the tine features on the deflector. The identified tine streams are observed to alternate with the narrow, downward directed streams formed by the slot in the deflector and visible at the lower elevation angles over the surface of the sphere. From the structure of the frame arm assembly, distinct shadow regions of minimal flux are visible on the initialization sphere at the 90° and 270° azimuthal locations. The reference frame arm discussed previously is the occurrence at 90°. It should be noted that a minimal amount of water is observed above the 100° elevation angle and the only water collected at the 80° location was a result of the frame arm feature obstructing the flow off the deflector and of negligible volume.

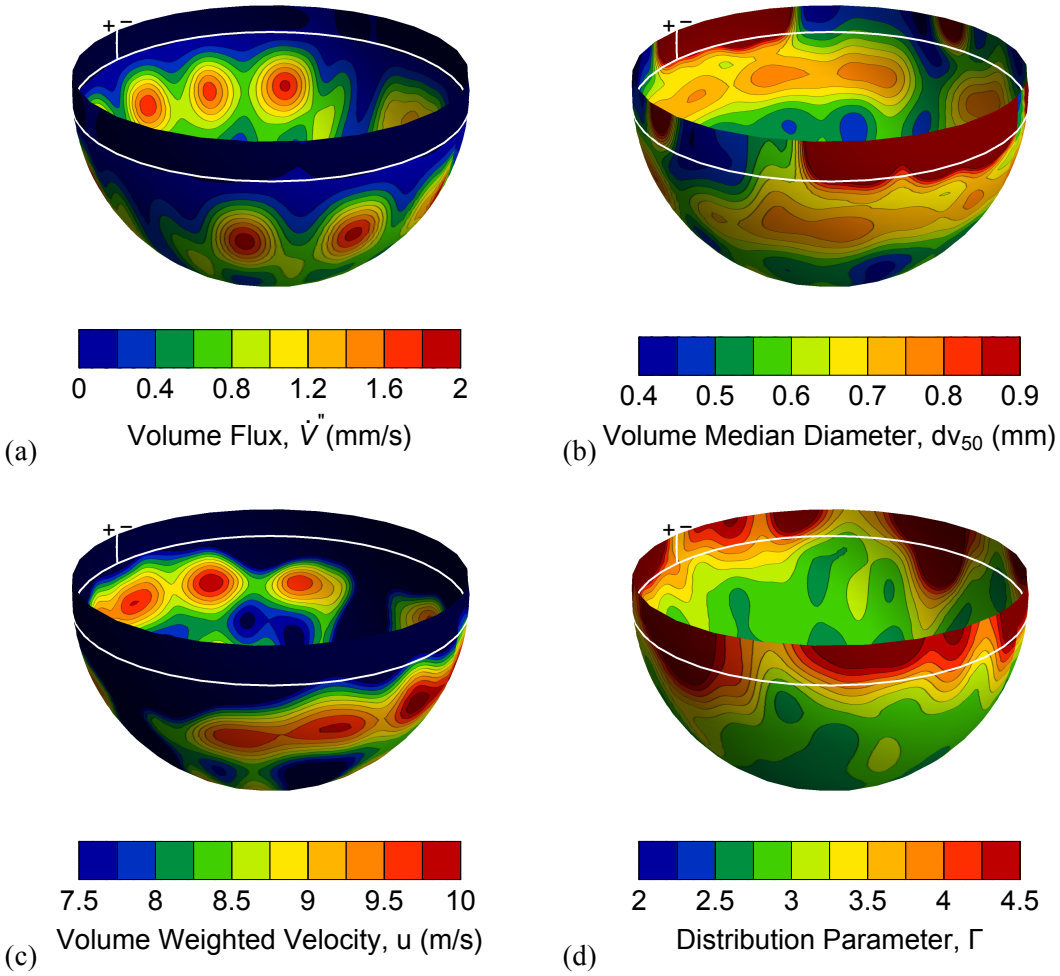


**Figure 9: Spatially-resolved 4S measurements of spray characteristics; (a) volume flux [mm/s]; (b) volume median diameter [mm]; (c) initial drop velocity [m/s]; (d) drop distribution parameter [27]**

To examine the volume flux measurement capability further, a point at $(\theta, \phi) = (150°, 165°)$ is selected. Flux measurement details at this point are presented in comparison to the local volume flux at a constant elevation angle, $\dot{v}''(\theta = 150°, \phi)$, as shown in Figure 10, as well as in contrast to local flux measurements at a constant azimuthal angle, $\dot{v}''(\theta, \phi = 165°)$, as shown in Figure 11.

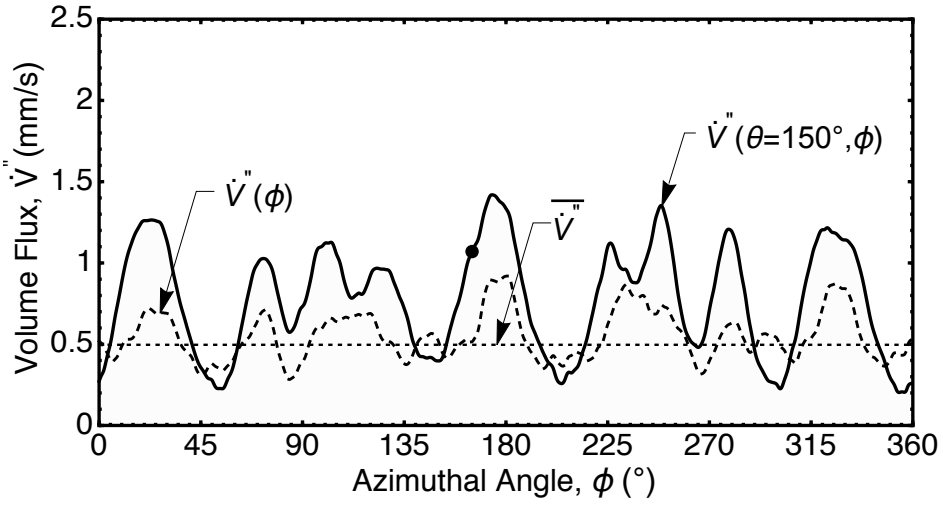


**Figure 10: Volume flux variation with azimuthal angle for $\theta = 150°$**

The local volume flux, $\dot{v}''(\theta = 150°, \phi)$, measured over all azimuthal angles at a constant elevation angle of $\theta = 150°$ is represented in Figure 10 by the thick curve. The average flux calculated as the $\sin\theta$ weighted average over all elevation angles at each azimuthal angle, $\dot{v}''(\phi)$, and the global average flux, $\overline{\dot{v}''}$, are presented on the same plot as the dashed curve and dotted line respectively. The global average flux was calculated from the total theoretical sprinkler flow rate divided equally over the initialization sphere area between the elevation angles of 80° and 180° as

$$\overline{\dot{v}''} = \frac{k\sqrt{P_s}}{r_m^2 \iint \sin\theta \, d\theta \, d\phi}. \tag{24}$$

A similar presentation is made in Figure 11 for: the local volume flux, $\dot{v}''(\theta, \phi = 165°)$, measured over all elevation angles at a constant azimuthal angle of $\phi = 165°$; the average flux calculated over all azimuthal angles at each elevation angle, $\dot{v}''(\theta)$; and the global average flux, $\overline{\dot{v}''}$. At $(\theta, \phi) = (150°, 165°)$ the local volume flux

(identified with a dot in the figures) was measured to be approximately 1.1 mm/s while the global mean volume flux was determined to be 0.5 mm/s. The local mean values across the elevation and azimuthal directions for the identified point are determined to be 0.52 and 0.78 mm/s respectively. The importance of spatial resolution in volume flux measurements of a sprinkler spray is observed from the non-negligible differenced in local and mean values in the presented figures.

The gradients of local volume flux across the elevation profile exceed those of the average flux calculated over all elevation angles while the opposite observation is made in the elevation angle profile in Figure 11. At $\theta = 150°$ the local flux is accurately represented by the global average flux at 11 points as estimated by the intersection of the two curves. In the elevation angle 3 points of intersection are identified for $\phi = 165°$. These occurrences are due to the periodicity of the measurement fluctuation through the mean value and are instantaneous points in space.

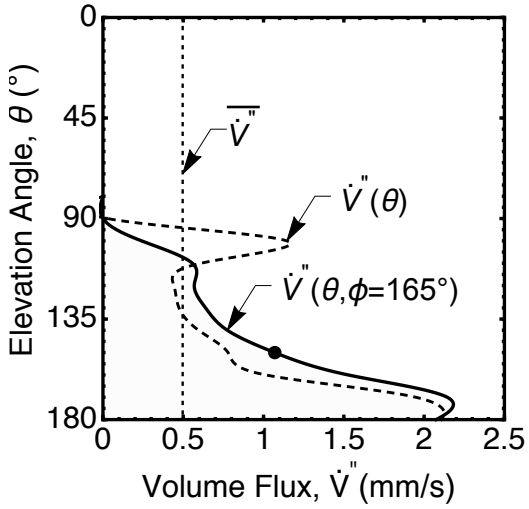


**Figure 11: Volume flux variation with elevation angle at $\phi = 165°$.**

To demonstrate the extent to which the mean approximations of volume flux are insufficient at predicting the local fluxes measured at each integer coordinate on the initialization sphere, we assume for the time being an acceptable error of ±10% for the volume flux estimation. Based on this ±10% tolerance in the flux value approximated by the mean, it was determined that the local volume flux is accurately represented by the global mean for 7.8% of the integer degree locations across $\theta = 150°$ and 3.3% over $\phi = 165°$. The sufficiency of the local mean approximations were also determined using the ±10% tolerance and are estimated to be 6.1% for $\dot{v}''(\phi)$ and 4.4.% for $\dot{v}''(\theta)$ and are presented in **Error! Reference source not found.**. Although the local ean approximation follows a similar trend in local maximum and minimum locations, the approximation by local mean is shown to be an insufficient representation of the spray. The lack of improvement to the local measurement estimation quality between the global and local mean approximations is notable in that it demonstrates that neither approach is sufficient for specification of the initial volume flux distribution on the initialization sphere at $(\theta = 150°, \phi)$ or $(\theta, \phi = 165°)$. An expanded discussion of the extent to which the global and local mean approximations are incapable of representing the spray is available in Appendix B.

**Table 3: Quality of local and global mean approximations**

| Approximation | ±10% Tolerance |
|---|---|
| $\dot{v}''(\phi)$ | 6.1% |
| $\overline{\dot{v}''}, \phi$ | 7.8% |
| $\dot{v}''(\theta)$ | 4.4% |
| $\overline{\dot{v}''}, \theta$ | 3.3% |

3.1.2. Optical Sphere Patternation

A typical approach for describing a sprinkler spray involves identification of either a characteristics or local drop size distribution. These distributions are commonly defined within the fire protection community using a median volume drop size, $d_{V50}$, and $\Gamma$, a distribution parameter indicative of spray uniformity. Although use of a single global drop size distribution would conveniently allow the spray to be described with just two parameters, the results of recent measurements indicate such an approach does not accurately capture the spatial variations in drop size and number.

A local drop size distribution taken at $(\theta, \phi) = (150°, 165°)$ containing nominally 1,200 quality droplet measurements was determined to have local $d_{v50}$ and $\Gamma$ values of 0.54mm and 2.8. In contrast, a global drop size distribution comprised of nearly 100,000 drop realizations produces global $d_{V50}$ and $\Gamma$ values of 0.57mm and 2.5, respectively. Although the detailed location selected compares well to the global spray parameters calculated, the $d_{V50}$ is observed to fluctuate between 0.38mm and 0.71mm across all azimuthal angles at $\theta = 150°$ while the calculated gamma spans values from 2.1 to 3.2. While $\Gamma$ does vary spatially, it should be noted that that calculated values of

gamma are largely consistent over regions of measurable flux and that areas of higher drop density have a slightly more consistent drop size distribution, higher $\Gamma$, than low density regions, exhibiting lower $\Gamma$.

Optical measurements of the spray confirm the previously observed spatial variability in drop characteristics. The distribution of the drop size parameters across all azimuthal angles at $\theta = 150°$ falls within ±10% of the global value for less than 46% of the discrete locations presented as degree increments on the spherical surface. Over the entire initialization sphere, measured parameters for the drop size distribution vary from the global value by less than ±10% over less than 39% of the measured locations on the initialization sphere. This indicates that a global drop size distribution parameter is not sufficient to characterizing the spray from a deflector based fire protection sprinkler.

Details of the local drop size characteristics at $(\theta, \phi) = (150°, 165°)$ are provided in Figure 12. The local volume flux based probability distribution and cumulative distribution of drop size demonstrate typical Log-normal Rossin-Ramler shape as seen in Figure 12a. The velocity correlation with drop size is shown in Figure 12b with the volume weighted drop velocity represented by the horizontal line.. It is clear even at this nearfield measurement location that drag has a large impact even on initial drop velocities; the smaller drops move much slower than the larger drops which move at a fraction of their Bernoulli velocity (15 m/s) at this location. Following Ren [11], it is assumed that drops move radially outward in the near field and all

measurements or drop size and velocity are taken in planes aligned with the spray's radial nature.

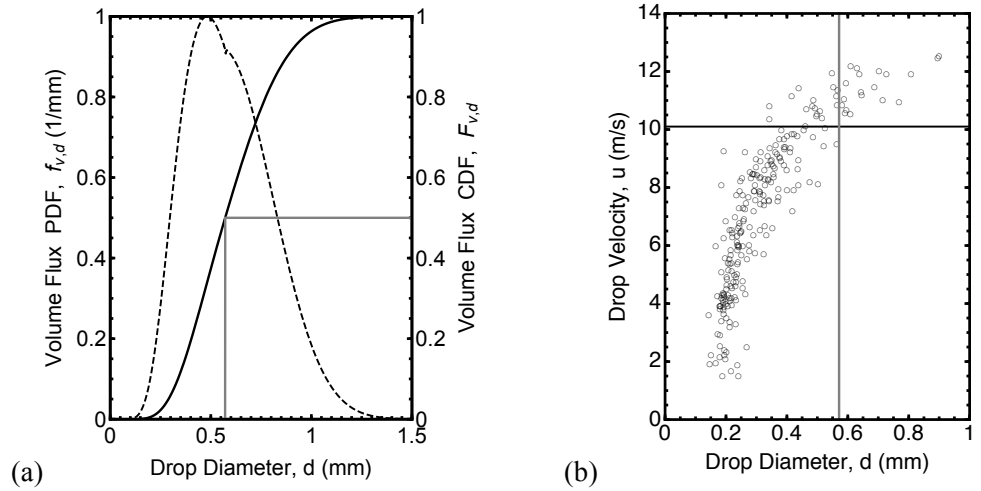


**Figure 12: Local spray characteristics; (a) drop size probability and cumulative distribution functions with dv50 identified; (b) drop size velocity correlation showing volume weighted mean velocity and dv50.**

### 3.1.3. Integral Line Patternation

The azimuthally averaged spray density on a plane 1 m below the sprinkler was examined with the integral line patternator of the 4S measurement device. The measured average volume flux profile with respect to radial position from the sprinkler is shown in Figure 13 and represents the radially averaged spray profile from the sprinkler of interest. Integrating the line patternation measurement over the radius of the spray collected accounts for 96% of the anticipated flow from the sprinkler. Integration of the function fit the measured volume flux over the full region of the spray would result in a cumulative volume fraction greater than unity indicating that a larger volume of water was collected than flowed through the sprinkler orifice. Further analysis should be conducted to evaluate the sufficiency of the collection cylinder

spacing in the integral line patternation device based on recent work conducted by Link [28].

General spray characteristics can be observed from the spray dispersion measurements presented in Figure 13. The sharp decrease in delivered density visible between 0.5 and 1.5 m is the result of the different sprays formed by the discrete slot and tine geometries on the sprinkler deflector. In this region the spray collected transitions from having a slot flow to a tine stream origin resulting in a longer throw and a less dense spray region.

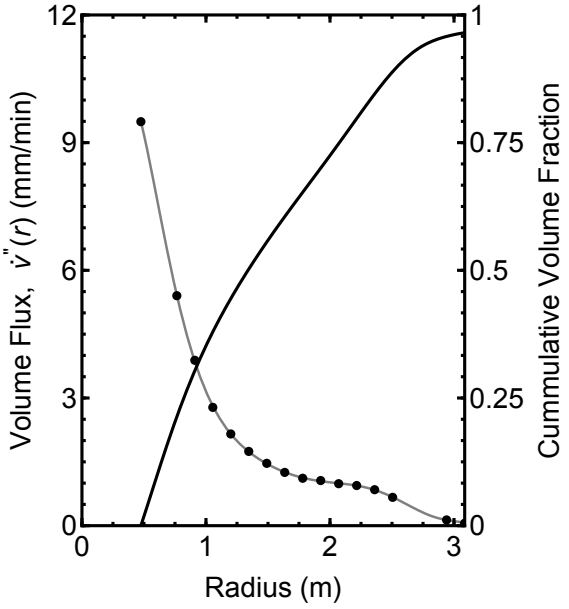


**Figure 13: Integral Line Patternation measurements for average radial profile and cumulative volume fraction; 4S measurements (dots), cumulative volume fraction (thick).**

To rapidly evaluate the quality of spray characterizations captured with the 4S, the integral line patternator can serve as a validation tool for the input parameters used in spray dispersion simulations. With the detailed drop characteristics available through

4S characterization measurements, the spray leaving the sprinkler and passing through a surface 1 m below the sprinkler can be modeled. Further discussion on spray characterization validation through CFD simulations and integral line patternation measurements are available in the section *3.3. CFD Integration*.

## *3.2. Error Analysis*

An error analysis was performed on measurements obtained from the various 4S subsystems. Potential error in test operation were determined to be primary contributors to measurement error. While error analysis for drop sizing was not strictly evaluated in this current work, the image processing parameters applied in these measurements were largely based on those from Ren [11] who reported repeatable characteristic drop sizes to within ±5%.

### 3.2.1. Mechanical Sphere Patternation

Flux measurements of the spray were first evaluated to baseline the mechanical sphere patternation measurement accuracy. Mass conservation over the initialization sphere surface was compared to a sprinkler flow reference. The data presented for volume flux was integrated over the spherical initialization surface,

$$\dot{v} = \iint \dot{v}''(\theta, \phi)\, r^2 \sin\theta \, d\theta \, d\phi. \tag{25}$$

Integral measurements were determined to typically fall within ±1% of the flow reference as calculated from test pressure and sprinkler k-factor.

Measurement repeatability was quantified for the flux-based mechanical patternation by examining multiple measurements of a sprinkler taken under identical

test conditions. Sprinkler inlet pressure was maintained in each test and the original sprinkler installation was preserved. Repeat measurements demonstrate excellent repeatability as illustrated in Figure 14. Based on multiple flux profile measurements, the positioning error was determined to be less than than ±1% with an associated flux error for the local flux measurement of less than ±2%.

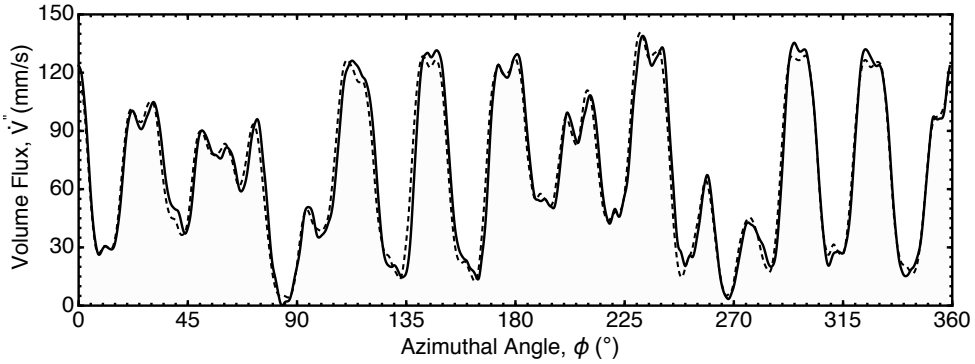


**Figure 14: Two azimuthal profiles from flux measurements at $\theta = 100^{o}$ [25]**

Future work related to the mechanical patternation measurements will include detailed analysis on measurement quality as affected by the measurement parameters of rotation time, collection cylinder size, and collection cap size. The tradeoff between measurement resolution and repeatability error will be theoretically developed and experimentally evaluated. Additional automation and standard test operating procedures are recommended to further reduce experimental error, specifically positioning error caused by sprinkler alignment and measurement error from proper collection cylinder sizing.

3.2.2. Integral Line Patternation

An azimuthally averaged spray density with respect to radial position delivered to a plane 1m below the sprinkler is calculated from the pressure differences using the total measurement time and cross sectional area of the collection cylinders. An equation fit to the average flux as a function of radius, $\dot{v}''_{R_i}$, and integrated over the range of the spray distribution is compared to the flow rate of the sprinkler, $\dot{v}$.

$$\dot{v} = 2\pi \int R_i \dot{v}''_{r_i} \, dR \tag{26}$$

For the sprinkler measurement presented in Figure 13, the integral line patternation measurement conserves 96% of the anticipated flow from the sprinkler over the measured floor patternation range. The error contribution from line patternator automation was also examined and determined negligible. The pressure transducer accuracy was determined to contribute negligible error through manufacturer calibration to 0.25% full scale. The repeatability error in measuring accumulated volume was determined to be ±0.15% using a 95% confidence interval over 126 measurements.

Based on the long azimuthal averaging time and the repeatability of the measurement approach, the radial local flux measurement errors are expected to be inconsequential. Overall line patternation measurement repeatability was estimated to be less than ±2% based on repeat measurements conducted under identical flow conditions. Systematic error in test operation including sprinkler alignment, collection cylinder positioning, and rotation time were determined to be negligible contributors

to observed test to test variations in the measured line patternation. Efforts are ongoing to address identified gaps and further reduce error through robust automation.

### *3.3. CFD Integration*

The spray characteristics captured with the 4S are sufficiently detailed for use in any spray modeling approach currently available. Based on preferred simulation speed and fidelity, computational fluid dynamics (CFD) software packages or simplified first order Lagrangian particle tracking algorithms may be applied to predict the spray density at any given surface using an identical 4S dataset. The complete spray summary captured with the 4S was applied in both numerical situations to first rapidly evaluate spray distribution and then in a detailed validation demonstration.

#### 3.3.1. Rapid Characterization Validation

A first order spray distribution model was applied to predict the wetting performance of a sprinkler at a plane 1 m below the sprinkler using the 4S spray characterization previously describe. By spatially averaging the simulation results, spray simulations can be directly compared to the integral line patternation data collected. The predicted and measured spray distributions shown in Figure 15 are observed to match well at the plane of interest over the range of radii measured.

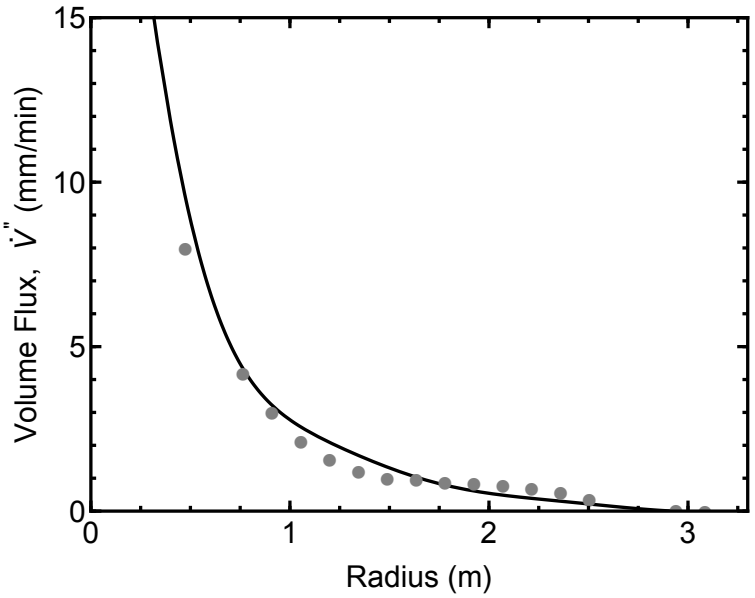


**Figure 15: Measured and predicted spray densities; measured with floor patternation (solid); predicted based on 4S characterization (dashed)**

3.3.2. Farfield Validation

With the complete set of spray measurements available from the 4S, the spatio-stochastic spray was initialized into a FireFOAM numerical simulation to predict the dispersion of the spray. First a candidate sprinkler was fully characterized using the described methodology to generate detailed local drop characteristics. Wetting of a plane 1.5m below the sprinkler was simulated and compared to highly resolved floor wetting measurements conducted by Link [28] for a quarter of the spray using the same sprinkler originally characterized with the 4S.

Previous attempts to integrate spray measurements into numerical simulations were limited by the availability of reliable local spray characteristics. With the spatially resolved spray characteristics available from 4S measurements, the intricacies of the spray are readily virtualized. It can be observed in Figure 16 that the sprinkler

dispersion predicted with the simulation matches the physically measured spray dispersion with a quality and agreement never before observed.

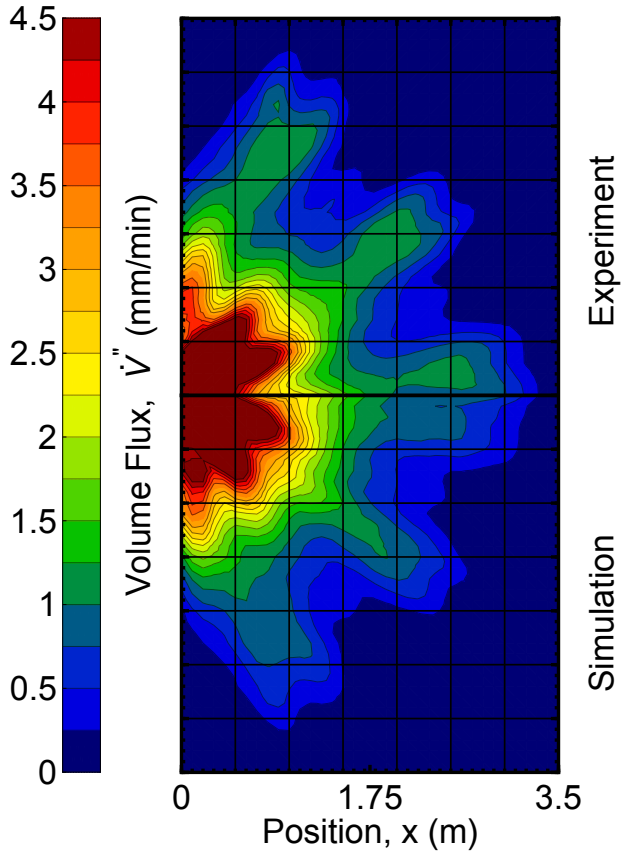


**Figure 16: Predicted and measured sprinkler dispersion at 1.5m for a quadrant of characterized sprinkler [25].**

The star-like shape of the measurements and predictions presented demonstrates the spatial variation in the structure of the spray and the ability of numerical simulations to predict these non-uniformities when provided with spatially resolved spray characteristics. The flow of water passing through the geometric slot features on the sprinkler is concentrated central to the sprinkler location. Distinct spray features extending from the spray core, forming the arms of the star pattern, originate

from the tine structures of the sprinkler. The spray predictions presented match the measured spray distribution to a degree never before reported.

The presented results for measured and predicted spray dispersion can be quantitatively analyzed by examine the azimuthal average volume flux distribution as a function of radial position from the sprinkler. The results of this approach, presented in Figure 17, are observed to match well over the region of spray measured. Both measured and predicted sprays demonstrate the non-uniformity of the spray and are observed to comprise more than a quarter of the sprinkler flowrate, identified by a cumulative fraction of expected flow greater than unity. The qualitative and quantitative agreement between the predicted and measured spray distributions presented is noteworthy and demonstrates the importance of quality spray measurements.

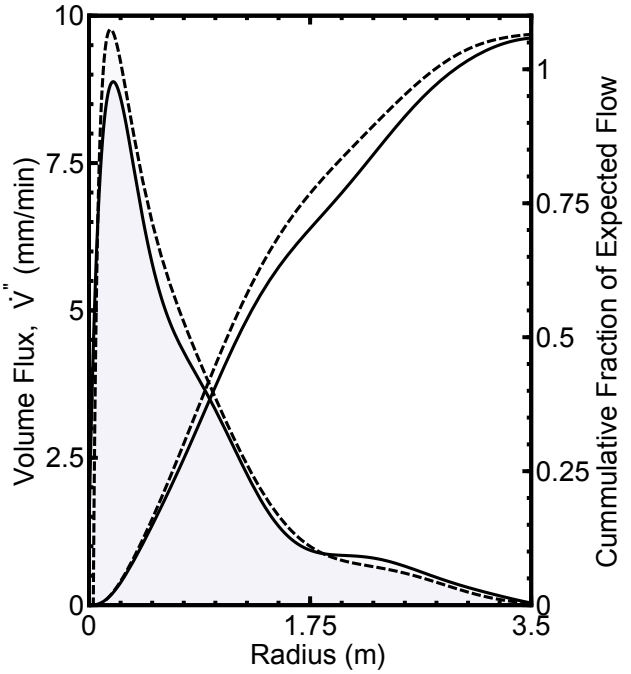


**Figure 17: Local and cumulative of measured (solid) and predicted (dashed) dispersion 1.5 m below the sprinkler.**

# Chapter 4: Conclusions

Spray characterization methodologies have evolved dramatically from freezing or collecting droplets in oil to physically capture and measure the drop sizes formed by fire protection sprinkler sprays. Recently, novel advancements in characterization capability have been limited by measurement methodologies compared to historical limitations associated with technological advancements. Until the development of the Spatially-resolved Spray Scanning System, detailed spray measurements were not readily accessible and required skilled laboratory personnel to manually align, capture, and process spray measurements for each feature of the sprinkler deflector.

A novel system for spatially-resolved sprinkler spray measurements was presented. The Spatially-resolved Spray Scanning System developed integrates cutting-edge diagnostic, automation and measurement synchronization, and an analytical framework to provide sprinkler spray characterizations with unprecedented spatial fidelity. The sophisticated spray measurement system developed utilizes state-of-the-art measurement capabilities to measure the spray in a continuous manner never before attempted and demonstrates excellent spray measurement accuracy and repeatability. The automated measurement approach applied requires limited technical skill to operate the system increasing measurement accessibility and quality while decreasing the time and cost associated with capturing spray measurements.

Volume flux measurements were determined to be ±2% and optical measurements estimated at ±5%. The demonstrated measurement capability enables further exploration of the spray formation phenomena and detailed investigation of the droplet interaction with the built environment and fire scenarios. The implementation of 4S characterizations in CFD numerical simulations was demonstrated to provide exceptionally good agreement between dispersion predictions and laboratory measurements reiterating the value of highly resolved initial spray characterizations for engineering analysis.

# Appendices

## *Appendix A. Applied Solutions - 4S Subsystem Details*

### A.1. Flow Control and Rotation

*Flow Control*

To control the inlet conditions of the sprinkler installed in the 4S measurement device, a dynamic bypass system was installed to control the injection pressure at the sprinkler by means of controlling the flow of water. A parallel arrange of two solenoid valves of different orifice sizes and a proportioning valve, Figure 18(a), were utilized to overcome the difficulties posed by a facility designed around a pump with a single speed motor and bypass a quantity of water from the pump directly to the drain. Flowrate and pressure measurements were taken on the sprinkler supply line of the 4S to measure the inlet flow and pressure conditions throughout the entire measurement process. These process measurements are taken upstream of the dynamic sealed coupling that allowed for the unique sprinkler rotation measurement approach as detailed in Figure 18(b).

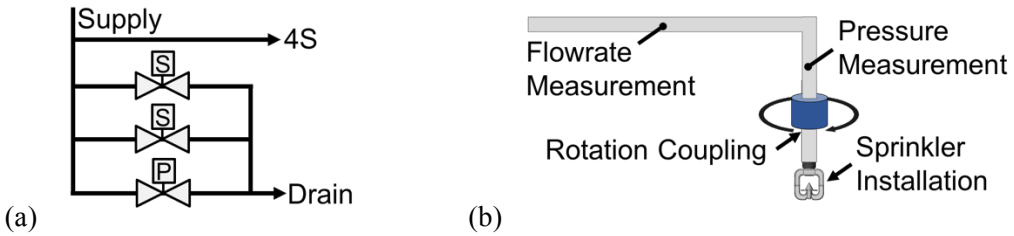


**Figure 18: Flow control system; (a) dynamic flow bypass configuration; (b) inlet flow measurement and rotation configuration.**

The parallel configuration of values in the design of this system allows various flow conditions to be achieved without imposing undue stress on the water supply

pump. The proportioning value, controlled with a PID algorithm, provides finite changes to the effective orifice size of the bypass drain based on pressure measurements while the two solenoid values provide course changes and expand the dynamic range of the proportion value as demonstrated in Figure 19.

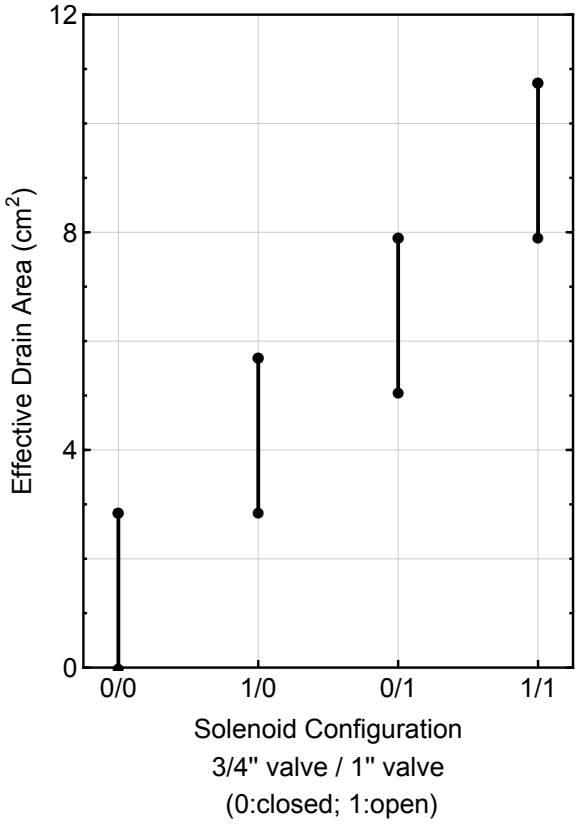


**Figure 19: Effective drain area span under available solenoid configurations.**

*Pressure Correction*

To accurately measure the injection pressure of the sprinkler it was necessary to calibrate the pressure loss between the measurement location and the orifice of the sprinkler. From equation (6) we know that the pressure setting is required to account for the friction loss in the length of pipe and fittings in addition to the head gained between the two locations,

$$P_S = P_T + P_{friction} + P_{minor} - P_{elevation}.$$

For the measurements report, flow measurements were conducted to characterize the losses with the exact fittings and couplings used during the installation of the sprinkler. The results from the focused flow testing indicated a pressure difference of approximately 1.1 psi (0.076 bar) between the pressure setting and the measured pressure. These measurements were taken at a set pressure of nominally 21 psi and based on the assumption that the the k-factor of the sprinkler is exactly the manufacture listed value of 2.3 GPM/psi$^{1/2}$. Since the actual value of the k-factor is allowed to fluctuate up to ±5% of the listed value over the listed range of the sprinkler, it is recommended that, when possible, future measurements of sprays be presented in terms of flowrate as opposed to operating pressure of the sprinkler. For more information pertaining to the calibration procedure applied for this testing the reader is directed to previous work conducted by Do [19].

*Sprinkler Configuration*

The sprinkler measured in this experimental investigation was installed in the pendent orientation. The 4S measurement device developed has the flexibility to measure not only pendant sprinklers, but also upright and sidewall sprinklers. There currently exists provision constructed into the 4S to easily remove and reposition the sprinkler mounting and rotational capabilities. A recent study using the 4S measurement device performed a complete characterization of an upright sprinkler with minimal alterations to the existing device infrastructure; only temporary rerouting of the water supply line was required to reposition the sprinkler.

## A.2. Mechanical Sphere Patternation

*Collection Cylinder Array*

The mechanical sphere patternation measurement subsystem contains 11 identical collection cylinder arrays designed to provide measurement flexibility and optimization. Each collection cylinder array is constructed of 8 different sized collection cylinders connected to a central manifold used to physically collect and measure the volume of water passing through the measurement region on the initialization sphere. The cylinder sizes were selected to populate the array based on an exponential growth in collection area. Each individual cylinder is isolated from the common manifold at a collection location by a quarter turn valve such that cylinder can be turned 'on' or 'off' to adjust the effective sensitivity of the flux measurement for each elevation angle. Figure 17 shows all the possible combinations of cylinders and the associated cross sectional areas for each with the red bars representing single collection cylinders. The total cylinder cross sectional area used for a specific test should be just large enough to collect all of the water delivered to a measurement location over the duration of approximately 1.25 rotations to account for startup and overlap durations in the measurement and reduce the risk of overflowing the cylinders and voiding the measurement.

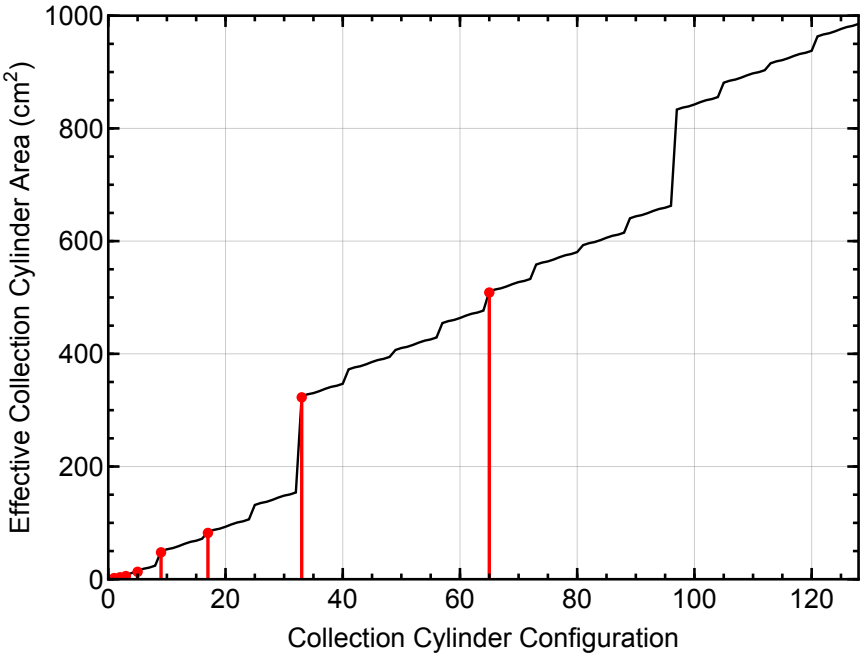


**Figure 20: Collection cylinder configurations and areas**

To rapidly drain the collection cylinders to a known water height a permanent reset drain was installed. The drain was positioned such that the reset water level was above the various valves and fittings used to connect the different cylinders within a single array and the location of the pressure measurement.

*Collection Cap Design Considerations*

Specialized collection caps were manufactured for to emulate a gore shaped region of the measured region of the sphere as discussed in Section 2.2.3. These collection caps were designed with several special considerations in mind based on the intended measurement location. First, all caps were constructed with a mitered edge to eliminate uncertainties with the actual cross sectional area of the probe. Additional consideration was given to the minimum width of the probed positioned at the 170° and 180° measurement locations. Should the cap design at these location be allowed to follow

the same $\sin(\theta)$ weighting as the other locations, the measurement width would approach zero at the 180° location and only partial drop diameters would be measured. To avoid the uncertainty associated with the collection of partial samples and the probability of collecting a valid sample in a finite measurement duration, a minimum width of at least 5 drop diameters was assigned to the measurement probe cap construction.

The measurement locations of 80° and 90° posed additional design challenges based on the physics of collection water that entered the measurement probes positioned horizontally or on a downward slope. To accurately collect the water reaching these measurement locations, the collection caps were manufactured to allow the probes to be positioned at the intended measurement location with the tubes connecting the probes to the collection cylinders positioned with at least a 5° slope downwards. With this configuration, all water entering the probe can be assured to reach the collection cylinders.

*Flux Data Alignment*

At the point in space where data collection is initiated, a seam in the measurements can be observed for measurements consisting of exactly one sprinkler rotation consistent with the single point repeatability of the measurement. To account for delays in data acquisition or errors associated with sprinkler alignment a smoothing technique utilizing redundant measurements of the first 30° of the sprinkler can applied to ensure that the initial azimuthal gradients of the spray pattern are resolved to same accuracy as those occurring later in the measurement process.

## A.3. Integral Line Patternation

The integral line patternation measurements detailed in Section 2.2.5 were taken using a series of 21 independent measurement locations. Applying a manifold concept from which all measurement locations are connected through an isolating quarter turn valve allows for a single pressure transducer to be used to measure pressures at 21 different locations. Prior to a test, all the cylinder isolation valves are opened in addition to a manifold drain valve. This allows all the cylinders to drain to an identical water height at which a baseline measurement can be taken. The drain valve and cylinder valves are all closed and exposed to the spray for a known duration. When the integral floor patternation measurement is initiated, pressure measurements from the single pressure transducer are continuously captured while individual cylinders are exposed to the manifold thus registering a pressure change on the transducer. After the complete measurement, the readings from the pressure transducer can be parsed and assigned to a radial position.

The line patternation measurements presented in this analysis were taken at a distance of 1 m below the sprinkler deflector. However, construction of the line patternation measurement subsystem is flexible and allows the measurement plane to be adjusted up to the height of the deflector. This additional feature of the 4S allows the spray dispersion to be interrogated in the near field and can be used to provide insight into sprays with reach longer than a 3.1 m radius at 1 m below the sprinkler.

## A.4. Optical Sphere Patternation

*Image Calibration*

Image calibration for the optical patternation measurements was conducted using a digital caliper. Reference images were taken with the calipers in the frame and illuminated by the diffuser. The images were then processed to define a pixel length scale based on the known measurement of the calipers. Calibration of the images was conducted prior to any optical measurements to ensure accurate drop size and velocity calculations.

*Image Processing Parameters*

In addition to the optical parameters presented in Section 0, several additional parameters are utilized in the processing of optical measurements. It was observed through the tests conducted that noise in the processed images could be dramatically reduced though the definition of the minimum shadowing parameter implemented in the first particle segmentation. This quantity defines an absolute threshold that the intensity of the inverted image must reach in order to be registered as a potential particle. Without an accurate definition of this parameter, images without particles may register larger quantities of small droplets due to inconsistencies with the diffuser illumination and particle saturation.

Additional noise control can be achieved through the definition of the high and low level thresholds used in the second particle segmentation. During this second segmentation, a long and short axis are identified for each threshold as well as a circle containing the same number of pixels and centered at the intersection of the two axis. Particle statistics including diameter, centricity, and location are calculated from the

average of the two sets of information for each particle identified. A processing parameter, called the maximal low level area, defines an acceptable ratio of the area calculated from the low level threshold comparted to that calculated from the high level threshold. A particle with a much larger area calculated from the low level threshold will have edges that do not appear as clear in the image as a particle with a much lower ratio. This parameter can be useful in tuning and defining the acceptable clarity of candidate droplet edges before proceeding with further analysis and processing.

In processing the velocity for each detected particle, an optional second pass was applied to the particle pairing with an initial shift adjusted based on the average shift identified in the first pass. During the second pass the search window size was reduced by half to provide a better estimate of the particle pairing. This allows the applied processing algorithm to narrow in on the most likely partner drop pair between the two images taken in a set.

*Appendix B.* *Global and Local Mean Approximation Sufficiency*

The quality of the local and global mean approximations of the spray compared to the mechanical sphere patternation measurements captured with the 4S was discussed in Section 3.1.1 as they pertain to a ±10% error tolerance. An expanded analysis was conducted to quantify and demonstrate the insufficiency of the two approximation methods, local and global means, based on the mean squared error and goodness of fit parameters typical to statistical analysis.

The mean squared error (MSE) of the agreement between a predictor and dataset is a cost function for which a minimum exists at an optimum fit. The MSE was evaluated for the local and global mean estimations for the volume flux distribution in the azimuthal and elevation angle profiles and are presented in Table 4. The MSE was determined to be 0.0017 $(mm/s)^2$ for repeated flux measurements and should be used as a metric for comparing the presented flux estimators. Further details pertaining to measurement repeatability are discussed in the error analysis section.

An additional metric used to evaluate the fit of the mean estimates was the reduced chi-squared statistic, $\chi_{red}{}^2$, to quantify goodness of fit. The $\chi_{red}{}^2$ parameter was estimated using the corrected sample variance of the spray measurement error. This parameter applied to a predictor of a dataset indicates a more sufficient model fit as values approach unity where the measurement and model fit is within the variance of the measurement error. These results are included in Table 4 and indicate that although the local mean approximation in Figure 11 yields the best fit to the experimental values, no sufficient generalization for volume flux can be made and

detailed spatially-resolved flux measurements are required to accurately represent sprinkler sprays.

**Table 4: Expanded quality of local and global mean approximations analysis**

| Approximation | ±10% Tolerance | Mean Square Error, MSE | Goodness of Fit, $\chi_{red}^2$ |
|---|---|---|---|
| $\dot{v}''(\phi)$ | 6.1% | 0.11 $(mm/s)^2$ | 62.2 |
| $\overline{\dot{v}''}, \phi$ | 7.8% | 0.19 $(mm/s)^2$ | 110. |
| $\dot{v}''(\theta)$ | 4.4% | 0.11 $(mm/s)^2$ | 20.5 |
| $\overline{\dot{v}''}, \theta$ | 3.3% | 0.17 $(mm/s)^2$ | 112. |

# Bibliography


[1] A. Lefebvre, *Atomization and Sprays*. Taylor & Francis, 1988.

[2] J. R. Lawson, W. D. Walton, and D. D. Evans, "Measurement of Droplet Size in Sprinkler Sprays," U.S. Department of Commerce, Feb. 1988.

[3] J. M. Prahl and B. Wendt, "Discharge distribution performance for an axisymmetric model of a fire sprinkler head," *Fire Safety Journal*, vol. 14, pp. 101–111, 1988.

[4] G. Grant, J. Brenton, and D. DRYSDALE, "Fire suppression by water sprays," *Progress in Energy and Combustion Science*, vol. 26, no. 2, pp. 79–130, Apr. 2000.

[5] H.-Z. Yu, "Invesitgation of Spray Patterns of Selected Sprinklers with the FMRC Drop Size Measuring System," *Fire Safety Science*, vol. 1, pp. 1165–1176, 1986.

[6] R. G. Bill, "Numerical simulation of actual delivered density (ADD) measurements," *Fire Safety Journal*, vol. 20, no. 3, pp. 227–240, 1993.

[7] S. Nam, "Development of a computational model simulating the interaction between a fire plume and a sprinkler spray," *Fire Safety Journal*, vol. 26, no. 1, pp. 1–33, 1996.

[8] D. T. Sheppard, P. D. Gandhi, and R. M. Lueptow, "Understanding sprinkler sprays: trajectory analysis," presented at the Fifteenth Meeting of the UJNR Panel on Fire Research and Safety, March 1-7, 2000, 2000, pp. 281–288.

[9] S. J. Walmsley and A. J. Yule, "A Study of the Sprays Produced by Fire Suppression Systems," presented at the Eighth International Conference on Liquid Atomization and Spray Systems, CA, USA, July 2000, 2000, pp. 1–7.

[10] N. Ren, A. Blum, Y. Zheng, C. T. Do, and A. Marshall, "Quantifying the Initial Spray from Fire Sprinklers," *Fire Safety Science*, vol. 9, pp. 503–514, 2008.

[11] R. Ning, "Advances in Characterizing Fire Sprinkler Sprays," 2010.

[12] L. A. Jackman, J. L. D. Glockling, and P. F. Nolan, "Water Sprays: Characteristics and Effectiveness," May 2003.

[13] J. Widmann, "Non-intrusive measurements in fire sprinkler sprays," *Fire Technology*, vol. 37, no. 4, pp. 297–315, Oct. 2001.

[14] A. D. Putorti Jr, “Simultaneous Measurements of Drop Size and Velocity in Large-Scale Sprinkler Flows Using Particle Tracking and Laser-Induced Fluorescence,” National Institute of Standards and Technology, 2010.

[15] J. F. Widmann, “Phase Doppler interferometry measurements in water sprays produced by residential fire sprinklers,” *Fire Safety Journal*, vol. 36, no. 6, pp. 545–567, 2001.

[16] N. Ren, H. R. Baum, and A. W. Marshall, “A comprehensive methodology for characterizing sprinkler sprays,” *Proceedings of the Combustion Institute*, vol. 33, no. 2, pp. 2547–2554, 2011.

[17] R. Ning, C. T. Do, and A. W. Marshall, “Knowing the Fire Sprinkler Spray,” presented at the FIRESEAT, 2011, pp. 37–46.

[18] A. Marshall, “Unraveling Fire Suppression Sprays,” *Fire Safety Science*, vol. 10, pp. 61–75, 2011.

[19] C. T. Do, “STREAM-WISE DISCHARGE CHARACTERISTICS OF PENDANT SPRINKLER SPRAYS,” 2009.

[20] X. Zhou and H.-Z. Yu, “Experimental investigation of spray formation as affected by sprinkler geometry,” *Fire Safety Journal*, vol. 46, no. 3, pp. 140–150, Apr. 2011.

[21] X. Zhou, S. P. D’Aniello, and H.-Z. Yu, “Spray Measurements of an Upright Fire Sprinkler,” *Fire Technology*, vol. 50, no. 3, pp. 457–482, 2012.

[22] X. Zhou, S. P. D’Aniello, and H.-Z. Yu, “Spray characterization measurements of a pendent fire sprinkler,” *Fire Safety Journal*, vol. 54, no. C, pp. 36–48, Nov. 2012.

[23] T. M. Myers and A. W. Marshall, “A description of the initial fire sprinkler spray,” *Fire Safety Journal*, vol. 84, pp. 1–7, Aug. 2016.

[24] D. T. Sheppard, “Spray Characteristics of Fire Sprinklers,” National Institute of Standards and Technology, 2002.

[25] S. J. Jordan, N. L. Ryder, and A. W. Marshall, “Spatially-Resolved Spray Measurements and Their Implications.”

[26] LaVision GmbH, “ParticleMaster Shadow,” 1105032, Dec. 2008.

[27] S. J. Jordan, “Spatially-Resolved Spray Measurements and their Implications,” *NFPA Conference and Expo*. pp. 1–1, 12-Jun-2016.

[28] E. D. Link, S. J. Jordan, T. M. Myers, P. B. Sunderland, and A. W. Marshall, "Spray dispersion measurements of a sprinkler array," *Proceedings of the Combustion Institute*, Aug. 2016.